ALBEDO AND SPECTRAL REFLECTIVITY OF THE GALILEAN SATELLITES OF JUPITER

Thesis by

Torrence Vaino Johnson

In Partial Fulfillment of the Requirements

For the Degree of

Doctor of Philosophy

California Institute of Technology

Pasadena, California

1970

(Submitted November 12, 1969)

ACKNOWLEDGMENTS

I wish to thank Dr. Bruce C. Murray for suggesting the Galilean satellites as interesting bodies for photometric study and for his steady encouragement and stimulating discussions during the course of this study. The aid of Dr. Thomas B. McCord is gratefully acknowledged. Many hours of observation together and many helpful discussions with him have been invaluable to my astronomical education. Also acknowledged is Dr. McCord's kind cooperation in the use of one of the filter sets used in this study and the use of reflectivity curves for the lunar mare and the bands of Jupiter before their publication.

Thanks also go to Mr. James A. Westphal and Dr. Andrew P. Ingersoll for carefully reading several stages of manuscript and providing valuable criticism. Several discussions with Drs. L. T. Silver and J. B. Adams about silicate reflectivities were very useful in interpreting the observations.

Finally, a very special acknowledgment is due my wife, Mary Eleanor, who earned her Ph. T. with flying colors while typing from my nearly illegible manuscript.

The author was supported by a National Aeronautics and Space Administration Traineeship for the duration of this investigation. Much of the research cost was supported by NASA Grant NGL 05-002-003.

ABSTRACT

An observational program designed to study the albedo and spectral reflectivity of the Galilean satellites of Jupiter was carried out during the 1969 opposition of Jupiter. A two-channel photoelectric photometer was used in conjunction with a high-speed pulse-counting data system to obtain and record the data. Narrowband interference filters ($\Delta\lambda \sim 0.02\mu$) were used with ITT FW-118 (S-1) and FW-130 (S-20) phototubes to obtain spectral reflectivity curves from 0.3μ to 1.1μ. The 24-inch telescope on Mt. Wilson was used for most of the work but the 60-inch instrument was used for some observations. The results of the observations were the following. 1) Spectral reflectivity curves from 0.3μ to 1.1μ for each satellite for many values of orbital phase angle and solar phase angle were obtained. 2) Spectral structure not resolved by broadband UBV work was found in J1's curve near 0.58μ and the similarity of the spectral reflectivity curves of J2, J3 and J4 was noted. 3) The very high geometric albedos of J1, J2 and J3, noted by Harris (1961), were confirmed. 4) The variation in brightness with orbital phase was confirmed for each satellite. 5) The spectral reflectivity was found to vary with the same period as the brightness, as indicated by UBV observations (Harris, 1961). 6) Variations in the spectral reflectivity of J1 and J2 beyond 0.6μ, not previously seen, were discovered. 7) The spectral form of the variation was found to be similar for each of the satellites, with the brighter side having a higher reflectivity in the blue and ultraviolet relative to 0.56μ than the darker side. 8) The eclipse brightening of J1 found by Binder and Cruikshank (1964) was confirmed at two wavelengths, 0.435μ and 0.56μ.

The conclusions drawn from these results and previous work are as follows. 1) J1 and J2 probably possess tenuous atmospheres while J3 and J4 probably do not. 2) All the satellites have significantly higher geometric albedos than Mercury, the moon or Mars, even allowing for large errors in the measurement of diameters. Of the satellites, J4 has a distinctly lower albedo and density than J1, J2 or J3. 3) The high geometric albedos and spectral reflectivities of the satellites can be explained by surfaces of silicate powders, possibly with considerable amounts of glassy material, having low opacities and some ingredient absorbing in the ultraviolet and blue, possibly Fe^{+++}. However, the possibility of surfaces of frost or some combination of frost and rock cannot be completely evaluated without further laboratory study. 4) The similarity in the variation of spectral reflectivity with orbital phase among the satellites suggests a similar cause for each. A simple model for J1's spectral variation suggests that some fraction of the bright side of J1 must be covered by a material with similar spectral reflectivity but higher albedo than the dark side (such as might be caused by particle size differences or a difference in the amount of the absorbing ingredient). The fraction of surface that must be covered and the exact form of the spectral reflectivity of the added material depends on the albedo chosen for this component. 5) The eclipse brightening observations at two wavelengths indicate that, if this effect is caused by the condensation of some volatile during the eclipse, the condensed material must have a very high geometric albedo, probably greater than unity. The simple model applied to the spectral variation, when applied to the eclipse brightening data, suggests that the condensed material is not gray in spectral character but has a lower reflectivity at 0.43μ than at 0.56μ.

TABLE OF CONTENTS

TABLE OF CONTENTS

LIST OF FIGURES

LIST OF FIGURES

LIST OF TABLES

I. INTRODUCTION

Knowledge of the four brightest satellites of Jupiter dates from the very beginnings of modern astronomy; they were first seen by Galileo when he turned his telescope on Jupiter. These satellites, often called the "Galilean satellites", are, after the earth's moon, by far the easiest satellite bodies to observe in the solar system, being bright enough to be seen with the naked eye but for their proximity to Jupiter.

The Galilean satellites are especially interesting to students of the solar system for two major reasons. First, they are part of the largest satellite assemblage in the solar system, often likened to a miniature solar system, revolving around the largest, and perhaps most interesting planet in the solar system. Second, their densities place them on the borderline between the so-called "terrestrial" and "Jovian" type planets (i.e., those with silicate or ice type densities, respectively).

Despite the relatively long time that the Galilean satellites have been observed, very little is known of these bodies compared to what has been learned of the moon and the planets. Both the bulk compositions and the nature of the surfaces of the satellites are unknown and the question of possible atmospheres is an open one. The lack of information concerning these characteristics is primarily due to the difficulties in observing the satellites close to the bright disk of Jupiter and due to the fact that only integral disk measurements of the satellites are possible (at opposition the satellites subtend approximately 1 arc second at the earth, the disks being discernible only through large telescopes under the

best of conditions). Also, the range of solar phase angle over which it is possible to observe the satellites is small (0 to 12 deg) due to Jupiter's distance from the earth and sun.

The most complete body of observational knowledge concerning the Galilean satellites is based upon the radiation reflected from their surfaces. Harris' article in The Solar System, Vol. III, (1961), presents a review of previous work and a compilation of some new results. The primary points of interest in this study are the following. 1) J1 differs significantly in U-B and B-V color from the other satellites, being one of the "reddest" objects in the solar system. 2) All four satellites show some variation in brightness with orbital position, the period of variation being equal to the satellite's orbital period. 3) The U-B and B-V color of J1 varies with the same period as its brightness and J2 and J3 show some evidence of variability in U-B color between their leading and trailing sides. 4) The geometric albedos of the satellites, especially J1 and J2, are abnormally high compared to other bodies in the solar system.

From previous studies of the reflectivity of the moon and laboratory studies of silicate powder reflectivities, it was felt that observing the satellites with increased spectral resolution ($\Delta\lambda \approx 0.02\mu$) and over an expanded spectral range (0.3μ to 1.1μ) would produce: 1) reflectivity curves with greater compositional information than the broadband UBV work; 2) information on the nature of the spectral changes with orbital phase, and 3) possible new spectral variations with orbital phase not resolved by the UBV observations. Furthermore, with the use of a double-beam photometer system, it was hoped that the accuracy of absolute photometric observations could be improved, particularly the values of the geometric albedos of the satellites.

II. OBSERVATIONS

Equipment. A double-beam photoelectric filter photometer developed for lunar reflectivity measurements by McCord (1968) was used to carry out the observations. Narrowband interference filters ($\Delta\lambda \simeq 0.02\mu$), spaced every 0.02μ to 0.05μ from 0.3μ to 1.1μ , were placed one at a time behind an aperture in the focal plane of the telescope. Table 1 shows the effective wavelengths for the filter sets used. Cooled ITT FW-118 (S-1 surface) and FW-130 (S-20 surface) photomultiplier tubes were used with a high-speed, dual-channel pulse-counting data system to detect and record the signals. The S-20 tube was used with the Vis and UV-Vis filter sets and the S-1 tube with the Vis-IR set.

Because of the necessity of obtaining data at many positions of the satellites, most of the observations were carried out with the 24-inch telescope on Mt. Wilson, where the required amount of observing time was available. Some of the data was taken with the 60-inch telescope on Mt. Wilson.

Techniques. The most difficult problem in observing the Galilean satellites is their proximity to a large, bright, extended object, Jupiter. Light from Jupiter scattered in the earth's atmosphere and in the telescope produces a field of brightness around the image of Jupiter in the focal plane. Thus, when the image of a satellite close to the planet is placed in the aperture, a considerable amount of scattered light from Jupiter also enters and is detected.

There are two basic methods of reducing the problem of scattered light. First, the aperture may be reduced to the minimum required to keep most of the light from the satellite in the aperture at all times. It was found that apertures

Table 1. Effective Wavelengths of Filters (Microns)

UV-Vis	Vis	Vis-IR
0.3060	0.4032	0.4060
0.3200	0.4224	0.4350
0.3400	0.4422	0.4660
0.3600	0.4612	0.4990
0.3860	0.4800	0.5320
0.4060	0.5040	0.5650
0.4350	0.5210	0.5980
0.4660	0.5403	0.6300
0.4990	0.5600	0.6640
0.5320	0.5782	0.6970
0.5650	0.6032	0.7300
0.5980	0.6180	0.7620
0.6300	0.6380	0.8000
0.6640	0.6637	0.8570
0.6970	0.6976	0.9000
0.7300	0.7204	0.9500
0.7620	0.7610	1.0000
0.8000	0.7990	1.0400
		1.0800

of 10 or 20 arc seconds (depending on seeing conditions) represented the best compromise between scattered light errors and errors due to losing part of the satellite signal from seeing changes, irregularity in telescope tracking, and the motion of the satellite. Second, the use of the double-beam photometer allows the scattered light component to be subtracted with some accuracy. As described more completely by McCord (1968), the double-beam photometer permits the alternate imaging (at 30 Hz) of two beams whose relative position in the focal plane may be adjusted in both separation and angular position. For use in observing the satellites, the second beam was placed at minimum separation (~1 mm in the focal plane, corresponding to ~20 arc sec at the 24-inch plate scale) at approximately the same distance from the planet as the satellite being observed. The signal from this beam was then subtracted in the data system from the satellite plus scattered light signal in the first beam, thus obtaining the signal from the satellite alone. Jupiter's semi-diameter, at opposition, is 23.43 arc sec. Observations of satellites were made as close to Jupiter as half an aperture (either 5 arc sec or 10 arc sec) and as far from Jupiter as 10 minutes of arc (J4's distance at mean opposition).

During an observing period, the following procedure was used. First, the photometer was set up with the first beam on the satellite and the second beam positioned to measure the sky brightness as described above. The filters were placed, one at a time, behind the aperture by a filter wheel, and the value of the signal was measured for a preset integration time in each filter. The integration time was chosen to yield enough counts in the filter with the lowest count rate to give a statistical error of ~10%, with the error in most filters being $\leq 1\%$. The signal in each beam, the difference between the two beams, the filter number and the total integration time in each filter were recorded by a Hewlett

Packard data printer. This sequence constitutes an "observation".

After an observation of a satellite, the telescope was either moved to another satellite or to a standard star, depending on the total time necessary to go through a filter set. Standard star observations were made at intervals of about 15 minutes when possible. Sometimes up to 30 minutes were required between observations of the standard star, particularly when using the infrared-sensitive tube (S-1), which, because of its low efficiency, required longer integration times. With the S-20 surface tube, it was common to take data on two satellites in a row before observing the standard star; the S-1 tube required switching back and forth to the standard star after every observation to ensure frequent enough standard observations.

III. REDUCTION OF DATA

Definitions. One of the most important photometric quantities associated with a planet is the ratio of the total light reflected from the planet to the total light incident on it. This ratio is defined as the Bond albedo, $A(\lambda)$, and is usually given as the product of two other quantities, the geometric albedo, $p(\lambda)$, and the phase integral, q. The geometric albedo is defined as the ratio of the planet's brightness at $\alpha = 0$ to the brightness of a perfectly diffusing disk with the same heliocentric position and apparent size as the planet, where α is the solar phase angle (sun-planet-earth). The phase integral is given by Equation 1:

$$1). \quad q = 2\int_0^{\pi} \phi(\alpha) \sin\alpha \, d\alpha$$

where $\phi(\alpha)$ is the phase law, the change of the planet's brightness with α, with $\phi(0) = 1$. q may also be a function of wavelength, but is usually taken to be constant. The geometric albedo, p, may be written in terms of the observed stellar magnitude of the planet and the stellar magnitude of the sun:

$$2). \quad \log p(\lambda) + \log \phi(\alpha) = 0.4\left[m_{\odot}(\lambda) - m_{planet}(\lambda)\right] + 2 \log \left(\frac{r\Delta}{R}\right)$$

where r = sun-planet distance in AU

Δ = earth-planet distance in AU

R = planet radius in AU = unit distance semi diameter in arc sec/206265

The difference between stellar magnitudes is defined by Equation 3:

$$3). \quad m_1 - m_2 = -2.5 \log \frac{F_1}{F_2}$$

where F_1 and F_2 are the fluxes outside the atmosphere from object 1 and object 2 respectively (Allen, 1963).

Another geometric factor of importance in dealing with the satellites is the orbital phase angle, θ. θ is measured counterclockwise around the satellite's orbit from the point of superior geocentric conjunction. This angle refers only to the earth-Jupiter line, so the same value of θ will always result in the same satellite-planet geometry being presented to an observer on the earth. If the satellite is synchronous with Jupiter, there will be one-to-one correspondence between this angle and the longitude of the subearth point on the satellite's surface. Since the satellites vary in brightness with their orbital period, it is assumed that they are synchronous. The term "rotational phase angle" will therefore be used interchangeably with "orbital phase angle" hereafter. Also, the terms "leading side" (θ<180 deg) and "trailing side" (θ>180 deg) will be used. For this study, θ was calculated by assuming circular orbits for the satellites (the eccentricities are all less than 0.001). Equation 4 gives θ at time t_0:

$$4). \qquad \theta = \left[\frac{t_0 - t_{sc}}{T_p} \right] \times 360 \text{ deg}$$

t_0 = observation time

t_{sc} = time of last superior conjunction

T_p = orbital period

Figure 1 shows the geometry schematically for the earth-sun-Jupiter plane (since the orbital inclinations to the ecliptic of Jupiter and all four satellites are less than 1 deg, no correction for aspect was made in any calculation).

For convenience, it is useful to define a quantity which is independent of the geometrical factors. This is the normalized reflectivity, $R(\lambda)$, given by:

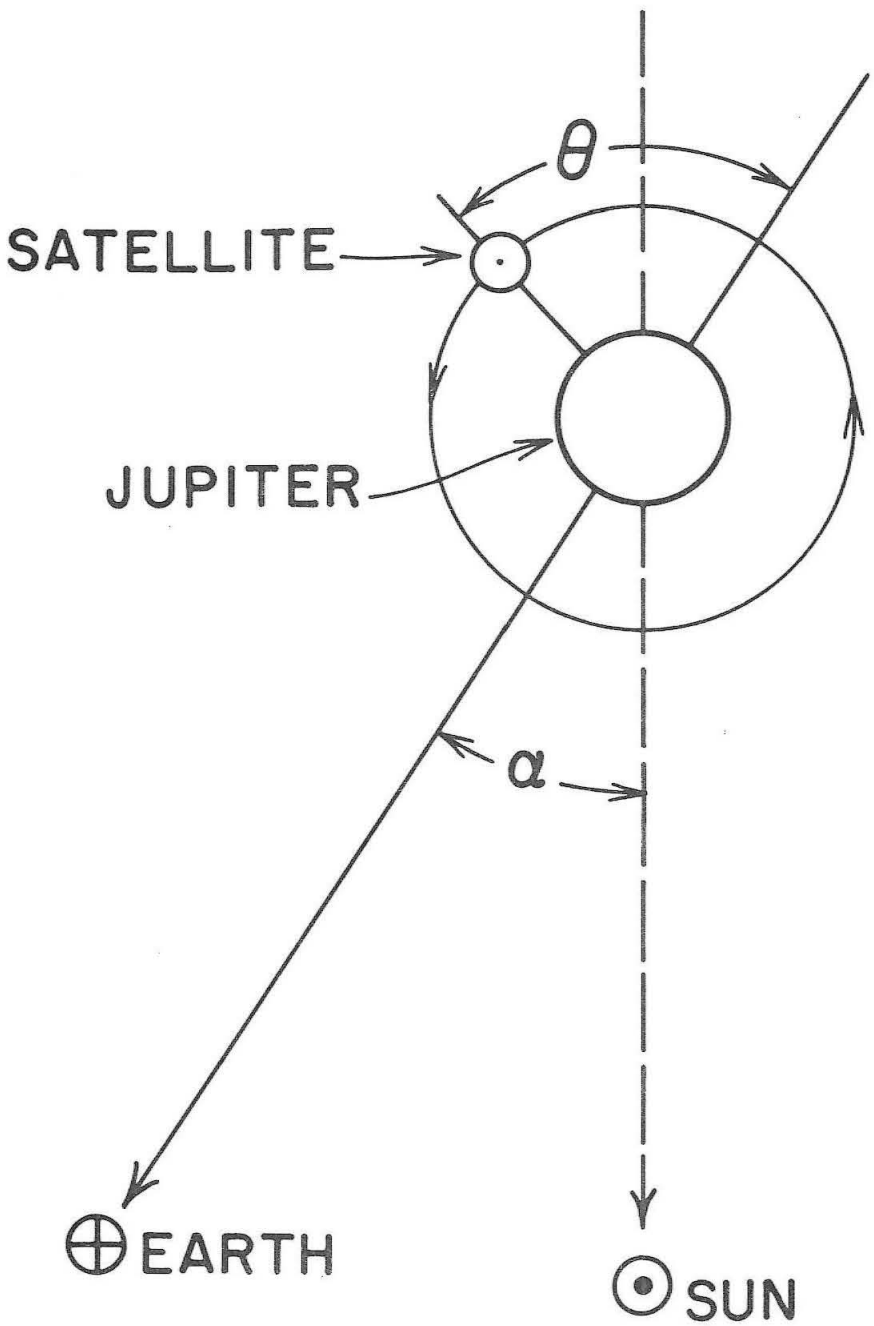

Figure 1. Schematic geometry of the earth-Jupiter-sun plane.

$$5). \quad R(\lambda) = \frac{p(\lambda)}{p(\lambda_0)}$$

where $\lambda_0 = 0.56\mu$ in this study.

From Equation 2, this becomes:

$$6). \quad \log R(\lambda) = 0.4\left[m_{\odot}(\lambda) - m_{\odot}(\lambda_0)\right] - 0.4\left[m_{planet}(\lambda) - m_{planet}(\lambda_0)\right]$$

From the definition of stellar magnitudes, Equation 3, $R(\lambda)$ may be written in terms of the normalized flux outside the atmosphere from the planet and the normalized solar flux:

$$7). \quad R(\lambda) = \left[\frac{F_{planet}(\lambda)}{F_{planet}(\lambda_0)}\right] \Big/ \left[\frac{F_{\odot}(\lambda)}{F_{\odot}(\lambda_0)}\right]$$

The normalized solar flux used in this study is given in Fig. 2. This curve was obtained by combining the solar flux given by Lambert (1967) from 0.4 to 1.1μ with the ultraviolet flux given in Robinson (1966). Robinson's curve agrees with both Lambert's and Allen's (1963) between 0.4 and 0.5μ.

Thus the important spectral information may be obtained from $R(\lambda)$, while the geometric albedo for all wavelengths may be obtained from $R(\lambda)$ and $p(\lambda_0)$. The method of obtaining $R(\lambda)$ from the observations will be discussed first since fewer assumptions are needed to calculate this quantity. Then the calculation of $p(\lambda_0)$ from observed quantities will be discussed.

Data Reduction. Unfortunately, the number of counts recorded by the data system in a given time through a given filter is not directly proportional to the flux outside the atmosphere, $F_{planet}(\lambda)$, which is needed for the calculation of $R(\lambda)$.

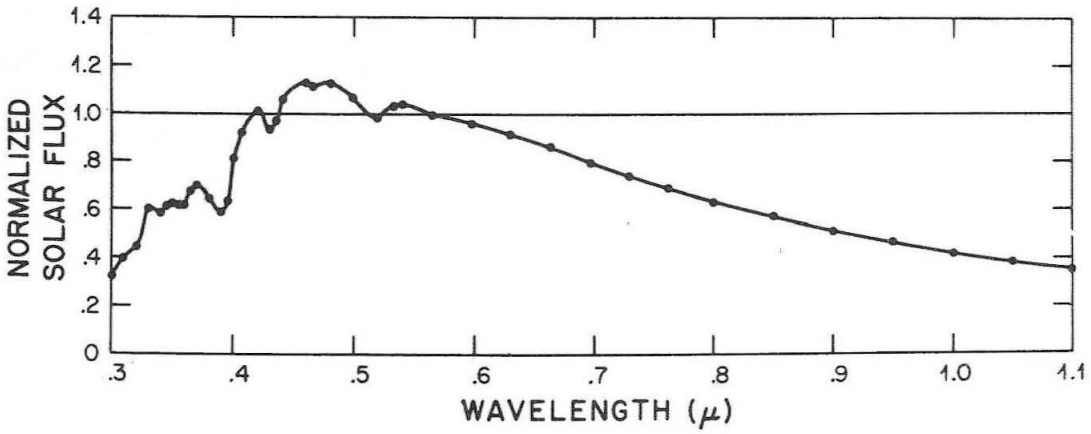

Figure 2. Normalized solar flux from Lambert (1967) and Robinson (1966).

$F_{planet}(\lambda)$ is modified by: 1) the atmosphere of the earth, and 2) the effect of the telescope, filter, detector combination. The measured flux, $f_{planet}(\lambda)$, can be written in terms of $F_{planet}(\lambda)$ as follows:

$$8). \quad f_{planet}(\lambda) = a(\vec{r}_1, \lambda, t_1)\, T(\lambda)\, F_{planet}(\lambda)$$

where $a(\vec{r}_1, \lambda, t_1)$ is the atmospheric transmission as a function of the planet's position in the sky, wavelength and time. $T(\lambda)$ is the telescope, filter, detector through-put function.

There are two basic ways to find $F_{planet}(\lambda)$ from $f_{planet}(\lambda)$. One way is to carefully calibrate $T(\lambda)$ and then measure the object at many positions and times in order to remove the atmospheric effect. This is a very exacting and time-consuming procedure. The second method is to compare the measured flux from the planet with that of another object, usually a star, measured through the same system and as nearly as possible at the same time and position in the sky. The ratio of these measured fluxes is given in Equation 9:

$$9). \quad \frac{f_{planet}(\lambda)}{f_*(\lambda)} = \left[\frac{a(\vec{r}_1, \lambda, t_1)}{a(\vec{r}_2, \lambda, t_2)}\right] \left[\frac{F_{planet}(\lambda)}{F_*(\lambda)}\right]$$

where $\vec{r}_1$, t_1 and $\vec{r}_2$, t_2 are the position and time of observation for the planet and star respectively. If the star's flux has been previously determined by the first method, $F_{planet}(\lambda)$ can be determined if the atmospheric functions can be dealt with.

In order to remove the atmospheric effect, it is first assumed that the variation due to position in the sky is directly proportional to the variation in air mass, which is given by the secant of the zenith angle, sec z, where one air mass is the atmosphere between the ground and object at zenith. By using a

standard star as close as possible to the planet, the error due to this assumption is minimized.

In practice, the removal of the sec z effect is accomplished by choosing $t_2 = t_*$, where t_* is the time when the star is at the same sec z as the planet at time $t_1 = t_s$. The flux observed from the star at this time, t_*, is taken from a plot of count rate vs time for the star. Such a plot was made for each filter on each night.

Figures 3 and 4 illustrate the above procedure for the 0.4612μ filter on 1 March 1969. If t_s is the time of observation of the planet, t_* is then found as shown in Fig. 4 from the sec z vs time curve and the value of the star's observed flux at this time is found from Fig. 3, which gives count rate vs time. Systematic deviations from a smooth variation in the star's flux at t_s can be taken into account if it is assumed that the same variation affects an entire area of the sky, including the position of the planet. With t_s and t_* chosen in this manner, $a(\vec{r}_1, \lambda, t_s)$ is approximately equal to $a(\vec{r}_2, \lambda, t_*)$ and:

$$10). \quad \frac{f_{planet}(\lambda)}{f_*(\lambda)} \simeq \frac{F_{planet}(\lambda)}{F_*(\lambda)}$$

During the observing program, the star, o Virgo ($\alpha = 12^h02^m39.7^s$, $\delta = +09^\circ 00' 38''$) was used as a standard (as shown in Fig. 4), since it was close to Jupiter and was of spectral class G5, close to that of the sun. All stellar coordinates given here are for epoch 1950. In order to determine $F_{o\ Virgo}(\lambda)$, o Virgo was measured relative to α Leo ($\alpha = 10^h05^m42.7^s$, $\delta = +12^\circ 12' 44''$). α Leo's flux has been measured by comparison to α Lyr, whose flux has been determined by the first method mentioned above (Oke, 1964; Code, 1960). The normalized flux curve for α Leo is given in Fig. 5. $R(\lambda)$ for the satellites was then determined from Equation 7 in the following form:

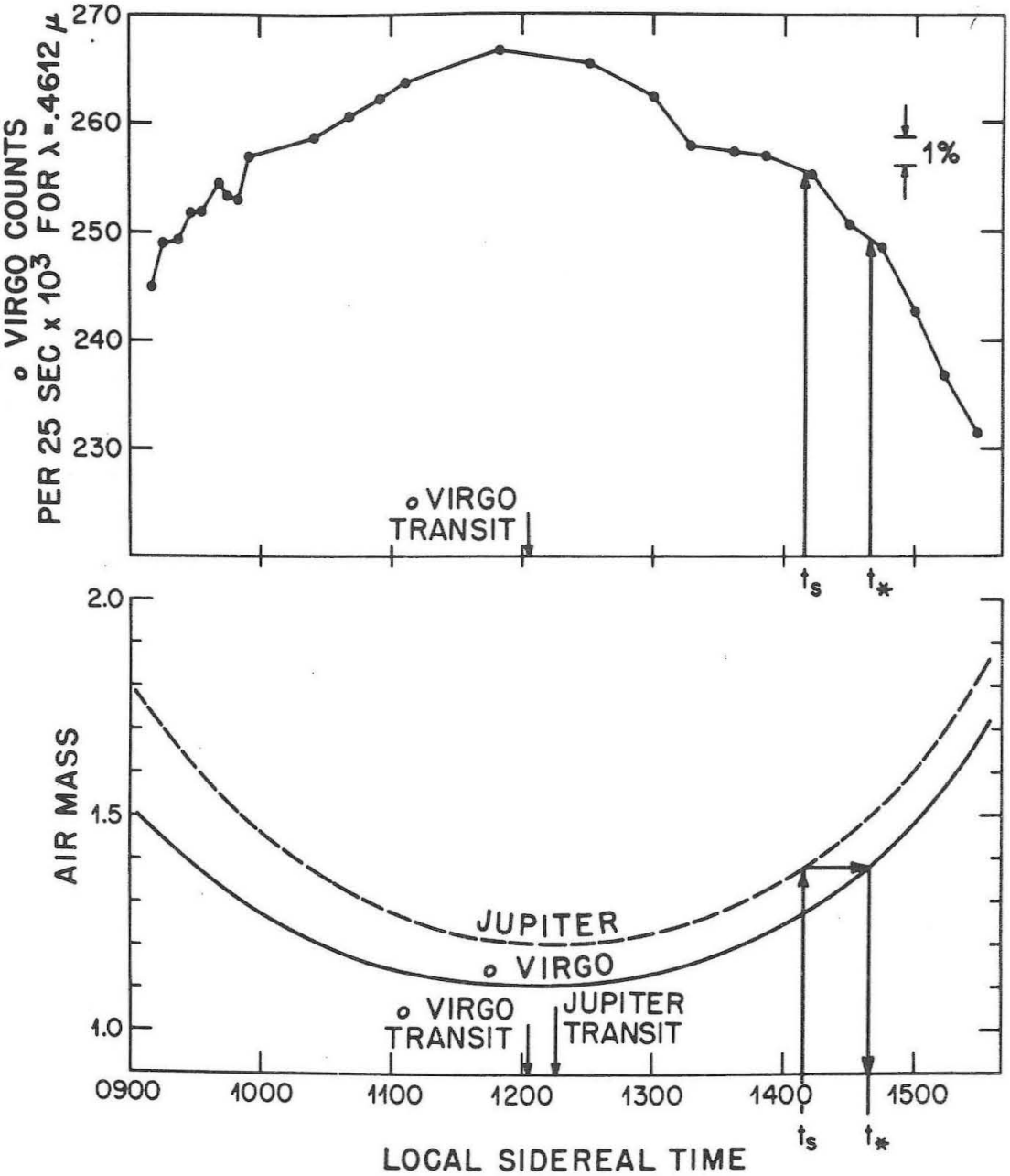

Figures 3 and 4. Measured flux vs time at 0.4612μ for the standard star, o Virgo, and air mass vs time for o Virgo and Jupiter on 1 March, 1969.

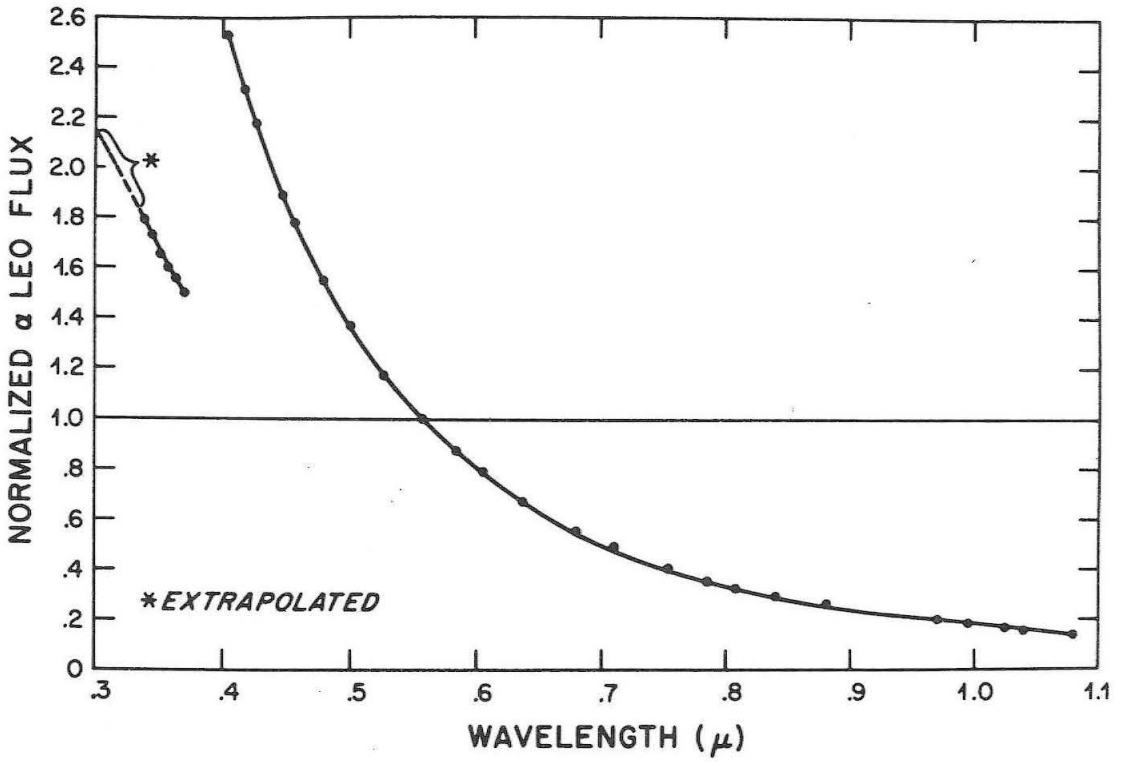

Figure 5. Normalized flux for α Leo from Oke (1964).

$$11). \quad R_{satellite}(\lambda) = \underbrace{\left[\frac{\left(\frac{f_{satellite}(\lambda)}{f_{o\ Virgo}(\lambda)}\right)\left(\frac{f_{o\ Virgo}(\lambda)}{f_{\alpha\ Leo}(\lambda)}\right)}{\left(\frac{f_{satellite}(\lambda_0)}{f_{o\ Virgo}(\lambda_0)}\right)\left(\frac{f_{o\ Virgo}(\lambda_0)}{f_{\alpha\ Leo}(\lambda_0)}\right)}\right]}_{\text{measured}} \times \underbrace{\left[\frac{\frac{F_{\alpha\ Leo}(\lambda)}{F_{\odot}(\lambda)}}{\frac{F_{\alpha\ Leo}(\lambda_0)}{F_{\odot}(\lambda_0)}}\right]}_{\substack{\text{calculated} \\ \text{from Fig. 2, Fig. 5}}}$$

The normalized spectral reflectivity, $R_{satellite}(\lambda)$, is one of the two major outputs of the observational program.

The second major output is the value of the geometric albedo at λ_0, $p(\lambda_0)$, from which $p(\lambda)$ at all wavelengths can be determined from Equation 5 and knowledge of $R(\lambda)$. The calculation of $p(\lambda_0)$ is complicated by the geometrical factors, $\phi(\alpha)$, r, Δ, and R of Equation 2 as well as by uncertainty in $m_{\odot}(\lambda_0)$, the absolute magnitude of the sun at 0.56μ. $p(\lambda_0)$ can be written, from Equation 2, as:

$$12). \quad p(\lambda_0) = \left[\frac{F_{planet}(\lambda_0)}{F_{\odot}(\lambda_0)}\right]\left(\frac{r\,\Delta}{R}\right)^2 \phi^{-1}(\alpha)$$

Writing this in terms of quantities measured in this study, calculated quantities, and assumed functions, Equation 12 becomes:

$$13). \quad p_{satellite}(\lambda_0) = \underbrace{\left[\frac{f_{satellite}(\lambda_0)}{f_{o\ Virgo}(\lambda_0)}\right]\left[\frac{f_{o\ Virgo}(\lambda_0)}{f_{\alpha\ Leo}(\lambda_0)}\right]}_{\text{measured}} \times \underbrace{\left[\frac{F_{\alpha\ Leo}(\lambda_0)}{F_{\odot}(\lambda_0)}\right]\left[\left(\frac{r\,\Delta}{R}\right)^2\right]}_{\text{calculated}} \underbrace{\left[\phi^{-1}(\alpha)\right]}_{\text{assumed}}$$

The first quantity in brackets is directly obtained from the observations. The second quantity must be calculated from the difference in magnitudes between α Leo and the sun by Equation 3. These magnitudes are obtained from previous photometry using the V filter of the UBV system, having an effective wavelength of 0.554μ. Although the passband of the V filter ($\Delta\lambda \simeq 0.1\mu$) is different from the passband of the 0.56μ filter used in the present study ($\Delta\lambda \simeq 0.02\mu$), the estimated error in determining $m_\odot$ is large ($\sim \pm 0.1$ mag.) and therefore V magnitude values were used in this study without correction for passbands. The $m_\odot$ chosen here is $m_\odot = -26.81 \pm 0.1$ mag. from Harris (1961), while $m_{\alpha\ \mathrm{Leo}} = 1.34$ mag. was taken from Oke (1964). These values result in:

$$14). \quad \frac{F_{\alpha\ \mathrm{Leo}}(\lambda_0)}{F_\odot(\lambda_0)} = (5.5 \pm 0.4) \times 10^{-12}$$

The third quantity in brackets in Equation 13 contains the distance of the planet from the earth, Δ, the sun, r, and the planet radius, R, all in units of AU. R must be found from published measurements, r and Δ are obtainable from the ephemeris. The radii of the satellites are difficult to measure accurately since they present very small disks ($\sim$1 arc sec) even at opposition. Various measurements of R using different techniques are discussed in Chapter IV, in the section devoted to the satellites' albedos.

The final factor, the inverse of the phase law can, in theory, be deduced from the change of the measured fluxes with solar phase angle. In the case of the Galilean satellites, the variation in brightness due to orbital phase makes the determination of $\phi(\alpha)$ difficult even over the small range of α's possible (0 to $\sim$12 deg). The procedure usually adopted is to assume a phase law in the form of Equation 15:

$$15). \quad \Delta m(\alpha) = -2.5 \log \phi(\alpha) = A\alpha + B\alpha^2 + \ldots\ldots$$

and to determine the coefficients from the data. The degree of coefficient which can be determined depends on the range of α. Only A was determined for the satellites in this study, as described in Chapter IV.

Sources of Error. The possible sources of error fall into two categories: those due to errors in the unreduced numbers and those due to the reduction process. In the first category are statistical errors due to a low number of detected photons and errors arising from the scattered light of Jupiter. Photon statistics should follow a Poisson distribution. For such a distribution, the statistical errors are proportional to $(N)^{-1/2}$, where N is the number of pulses counted. N is smallest and the errors are largest in the ultraviolet and infrared regions. In the ultraviolet, the solar flux curve is decreasing rapidly and atmospheric absorption is increasing; both effects reduce the number of photons reaching the detector. In the infrared, the quantum efficiency of the S-1 photosurface, already much lower than for the S-20, is dropping very rapidly, reducing the number of photons counted. The integration time was chosen to compromise between getting adequate statistics in the infrared and UV filters and being able to cycle the filters often enough to provide good extinction curves. For the S-20 surface, 2.5 sec/filter integration time was used on the 24-inch telescope; for the S-1 surface, 5 sec/filter was used. The resulting statistics yielded statistical errors of 10% or greater, for a single observation in the first one or two filters of the UV-Vis and for the last one or two of the Vis-IR filter set, with errors from this source running 1% or less over the majority of the filters.

The amount of scattered light received by a 20-arc sec aperture placed 1 or 2 Jupiter diameters from the planet was about 20-30% of the satellite signal in the blue, and approximately 10% toward the red and infrared. At 3 or more diameters separation, the scattered light was typically down by a factor of 2

from the above figures. Trials of observing the scattered light at various positions indicated that the subtraction procedure outlined in Chapter II resulted in an error for a given observation of a few percent of the satellite signal. Independent positioning of the second beam for each satellite observation during a night provided some cancellation of systematic errors due to mechanical positioning, since the second beam should then be placed too close, as often as too far, from the planet. Comparison of data taken at nearly the same distance from the planet, but at different orbital positions, indicates that the overall error due to scattered light in averaged results is probably on the order of 1%.

In the second category of errors, those due to the reduction process, are errors arising from the extinction corrections and from the choices of flux curves for the standard star and for the sun. The uncertainty in extinction is particularly severe in the blue and ultraviolet, where the changes during the night are large due to Rayleigh scattering (the flux change from 2-1/2 air masses to transit at approximately 1 air mass being ~30% at 0.4032μ). In the infrared, the secular changes become as large as the air mass effect and make the accurate choosing of an extinction correction difficult. Thus, these errors are largest where the statistical errors are also large. This combination probably contributes most of the scatter seen in the data during a single night.

Comparison of reflectivity curves obtained on different nights is a good check on the accidental errors due to extinction. Systematic changes in the atmosphere during a night, such as a general decrease in transmission over one part of the sky, might not be compensated for by the extinction correction, but such a change would not be expected to occur in exactly the same way on repeated nights over a period of a month. The agreement of reflectivity curves

taken on different nights indicates that such effects are not producing errors of more than a few percent.

The errors possible in the choice of solar and standard star flux curves are systematic in nature. An error in slope of one of these flux curves would simply introduce a proportionate error in the slopes of the reflectivity curves of the satellites. A confirmation that there are no gross errors of this sort is provided by the agreement in slope of the curves found in this study with the UBV curves from Harris (1961), where an entirely different set of standard stars was used and the UBV color of the sun was used instead of the solar flux curve chosen in this study.

Systematic errors in brightness between the sun and standard stars were discussed above and found to be of the order of at least 0.1 mag. in the sun's V magnitude. The effect of this type of error is to alter the values of the geometric albedos of the satellites. Recalling the definition of geometric albedo, it is easily seen that the percentage change in geometric albedo is given by:

$$16). \quad \frac{\Delta p}{p} = 0.4 \delta m_{\odot} \ln 10 = 0.92 \delta m_{\odot}$$

where $\delta m_{\odot}$ is the error in magnitudes in the V magnitude of the sun.

The scatter in reflectivity data for several observations of a satellite during one night gives an indication of the magnitude of random and short period errors such as those due to Poisson statistics, different settings of the scattered light subtraction beam and short term atmospheric effects. An estimate of this scatter was made for each night for each satellite by averaging all the reflectivity observations of each satellite for that night and then calculating the standard deviation of the average value given by:

17). $$\sigma_{avg} = \left[\frac{\Sigma \Delta^2}{N(N-1)}\right]^{1/2}$$

where $\Delta = R(\lambda) - R_{avg}(\lambda)$ and N is the number of curves averaged. This procedure neglects changes due to changes in the orbital phase angle, θ, over a night. With the possible exception of J1, the variation of the reflectivity curve due to changing θ over one night was of the same order as, or smaller than, the scatter due to the above. The average value for the ratio of each satellite to the standard star at the normalizing wavelength and the σ_{avg} associated with it were also calculated.

IV. RESULTS

Chapter IV presents the results of the observational program carried out during the 1969 opposition of Jupiter. These results are presented in the following order:

Section 1). Standard Star. This section contains the normalized ratio of o Virgo to the sun as a function of wavelength, and the stellar magnitude of o Virgo at 0.56μ.

Section 2). Satellite Reflectivites. Section 2 contains the average $R(\lambda)$ curves for each satellite from 0.3μ to 1.1μ.

Section 3). Changes in Spectral Reflectivity with Orbital Phase. This section gives the variation, as a function of θ, of $R(\lambda)$ at several wavelengths and the variation in $R(\lambda)$ between two θ values as a function of wavelength.

Section 4). Brightness Variations with Solar Phase Angle and Orbital Phase. Section 4 treats the phase laws, $\phi(\alpha)$, and the variation in mean opposition magnitudes of the satellites with θ.

Section 5). Geometric Albedo and Density. Section 5 treats the uncertainty in these quantities due to uncertainties in radii determinations.

Section 6). Bond Albedo and Phase Integral. This section covers several methods of estimating the phase integral, q, for each satellite, and the various resulting Bond albedos.

Section 7). Eclipse Brightening. Section 7 presents data taken at 0.435μ and 0.56μ of an eclipse reappearance of J1.

Standard Star. The standard star, o Virgo, was measured relative to α Leo on 4 nights throughout the observing program. Table 2 gives the date, filter set and number of observations of o Virgo for each of these nights. These measurements were carried out with both of the phototubes used over the total range of the filter sets, 0.3μ to 1.1μ. Figure 6 shows the resulting normalized ratio of o Virgo to the sun, calculated using Oke's flux curve for α Leo (Fig. 5) and the solar curve (Fig. 2). These values for each filter are given in Table 3.

Table 2. Log of o Virgo Observations

Date	Filter Set	Number of Observations per Night
03/04/69	Vis	5
03/22/69	Vis	3
04/17/69	UV-Vis	3
04/22/69	Vis-IR	3

Since the flux of α Leo is uncertain at 0.386μ, due to a discontinuity in α Leo's flux curve, the value shown in Fig. 6 for this wavelength has been chosen to give a smooth curve between 0.36μ and 0.406μ. The high value of the star-solar ratio for 0.3200μ appears to result from some systematic error. Satellite reflectivities obtained by using this curve also show an anomalously high value for this filter, while direct ratios of one satellite against another show a smooth variation in this region. As it seems unlikely that a spectral feature of this type would appear in both satellite and stellar curves in the same way, an error in either the assumed flux of α Leo or the sun is indicated. All solar curves used give approximately the same shape for the solar curve in this part of the ultraviolet. However, the flux of α Leo was not measured by Oke below 0.339μ. The error, then, probably lies in the assumed extrapolation of α Leo's flux. The

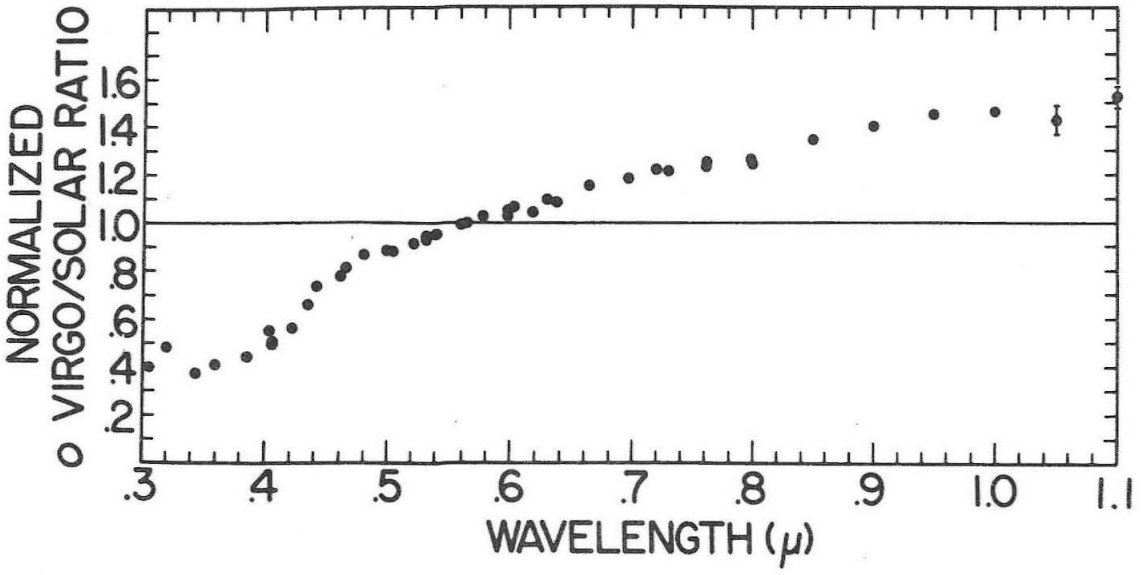

Figure 6. Normalized o Virgo/solar ratio. The points shown are an average of several observations and the standard deviation of the average is shown where it is larger than the diameter of the data point.

Table 3. Normalized o Virgo/Sun Ratio

UV-Vis		Vis		Vis-IR	
λ_{eff}	Ratio	λ_{eff}	Ratio	λ_{eff}	Ratio
0.3060	0.398	0.4032	0.554	0.4060	0.502
0.3200	0.487	0.4224	0.575	0.4350	0.664
0.3440	0.372	0.4422	0.745	0.4660	0.818
0.3600	0.416	0.4612	0.794	0.4990	0.892
0.3860	0.449	0.4800	0.882	0.5320	0.937
0.4060	0.496	0.5040	0.888	0.5650	1.000
0.4350	0.664	0.5210	0.925	0.5980	1.045
0.4660	0.818	0.5403	0.960	0.6300	1.095
0.4990	0.892	0.5600	1.000	0.6640	1.156
0.5320	0.937	0.5782	1.035	0.6970	1.184
0.5650	1.000	0.6030	1.074	0.7300	1.216
0.5980	1.045	0.6180	1.058	0.7620	1.254
0.6300	1.095	0.6380	1.102	0.8000	1.246
0.6640	1.156	0.6637	1.147	0.8570	1.341
0.6970	1.184	0.6976	1.199	0.9000	1.404
0.7300	1.216	0.7204	1.247	0.9500	1.450
0.7620	1.254	0.7610	1.274	1.0000	1.464
0.8000	1.246	0.7990	1.266	1.0400	1.425
				1.0800	1.523

possibility of a similar error in the 0.300μ points also exists since the same extrapolation was used.

The average value for the ratio of o Virgo to α Leo at 0.56μ was found to be 0.0866±0.0012. This corresponds to a magnitude of 3.996±0.015 (taking the magnitude of α Leo as 1.34 from Oke), although it must be remembered that this is not strictly a V magnitude difference since the filter passbands used are much smaller than those of the V system filters.

Satellite Reflectivities. The bulk of the data taken is in the form of normalized reflectivity curves, for this function contains all of the spectral information, and such curves for different objects and different nights may be directly compared. Table 4 presents a log of observations, listing those nights which were good enough to produce reflectivity curves with a scatter of a few percent or less. The solar phase angle, filter set, the satellites observed, the orbital phase angle for each satellite, and the number of observations for each satellite are given in succeeding columns. It will be noted that the UV-Vis and Vis-IR filter sets were not available during the earlier portions of the program. As a result, the total coverage in terms of orbital position was not as good for the spectral regions covered by these sets. J1 was observed directly with the UV-Vis set only for θ>180 deg. However, it was possible to recover some UV-Vis data for θ<180 deg from relative (J1 vs J4) measurements.

Figure 7 shows a composite normalized reflectivity curve for each satellite from 0.3μ to 1.1μ. These were formed by combining curves taken with the different filter sets but at nearly the same orbital phase angle. The visible region of the curves is taken from one night for each satellite; the UV and IR portions, because of the larger errors in one night's observation, are averages of all observations of each satellite, for one side of the satellite. The designations "leading"

Table 4. Log of Satellite Observations

Date	α (deg)	Filter Set	Satellites Observed	θ (deg)	Number of Observations per Satellite
03/01/69	4.17	Vis	J1	254	9
			J2	262	6
			J4	320	8
03/04/69	3.42	Vis	J1	125	6
			J2	203	2
			J3	146	3
			J4	25	2
03/05/69	3.23	Vis	J1	320	1
03/10/69	2.25	Vis	J1	278	8
			J2	88	4
			J3	88	6
			J4	153	4
03/11/69	2.05	Vis	J1	121	9
			J2	195	2
			J3	139	8
			J4	174	3
03/22/69	0.0	Vis	J1	209	4
			J2	223	7
			J3	330	3
			J4	55	7
03/23/69	0.51	Vis	J1	35	5
			J2	320	6
			J3	15	8
			J4	74	10
03/26/69	1.08	Vis	J1	250	4
			J4	137	3
04/10/69	4.00	Vis	J1	93	7
			J2	340	2
			J3	208	4
			J4	104	6
04/11/69	4.18	Vis	J1	275	4
			J2	83	2
			J3	252	2
			J4	124	4

Table 4. Log of Satellite Observations (Contd)

Date	α (deg)	Filter Set	Satellites Observed	θ (deg)	Number of Observations per Satellite
04/13/69	4.55	Vis-IR	J1	325	3
			J2	295	2
			J4	168	4
04/16/69	5.09	UV-Vis	J1	228	6
			J2	235	5
			J3	148	6
			J4	232	6
04/17/69	5.26	Vis-IR	J1	75	2
			J2	339	1
			J3	202	1
			J4	256	2
04/18/69	5.43	UV-Vis	J1	273	5
			J2	77	2
			J3	250	2
			J4	277	5
04/20/69	5.78	Vis-IR	J1	238	2
			J4	316	1
04/21/69	5.94	Vis-IR	J1	152	2
			J2	19	1
			J3	41	3
			J4	340	3
04/22/69	6.10	Vis-IR	J1	340	2
		UV-Vis	J2	118	2
		"	J3	90	2
		"	J4	4.4	1
04/29/69	7.18	UV-Vis	J1	334	4
			J2	105	6
			J3	82	7
			J4	154	9
05/12/69	8.82	Vis-IR	J1	100	4
			J2	340	1
			J3	152	1
			J4	75	3
05/13/69	8.92	Vis-IR	J1	300	3
			J2	79	1
			J3	63	1
			J4	96	3

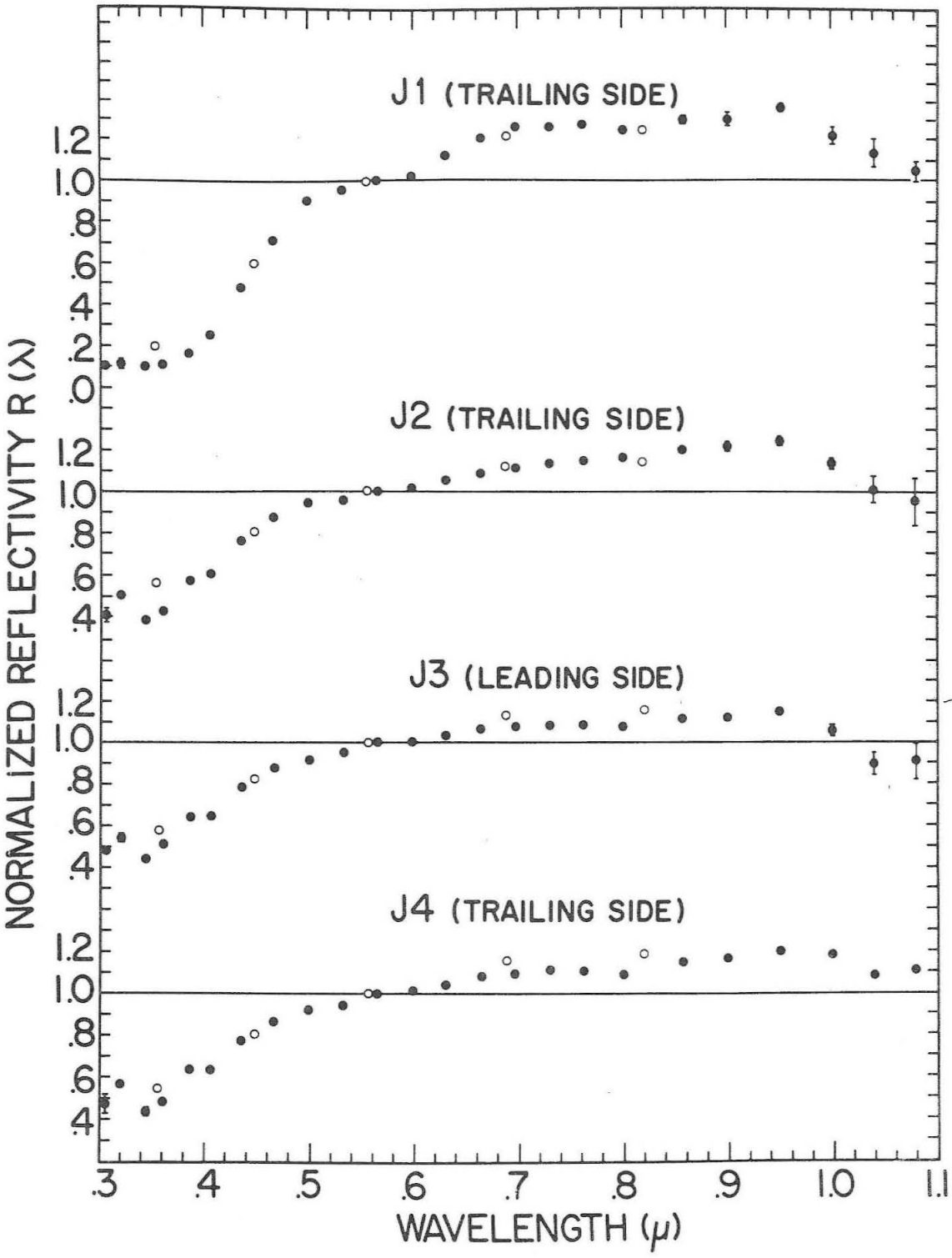

Figure 7. Normalized spectral reflectivity of the satellites. The data shown represent averages of several nights' observations; the standard deviation of the average is shown where larger than the diameter of the data point.

(θ<180 deg) and "trailing" (θ>180 deg) are included on the graph. For Fig. 7, the side shown was chosen for which the greatest number of observations in the UV-Vis set existed. The error bars shown are the standard deviation of the average. If the error is smaller than the diameter of the point, no error bar is shown. The large open circles are the UBVRI reflectivities taken from Harris (1961). As mentioned in Chapter III, Sources of Error, the agreement in overall slope between the narrowband data and the UBVRI points indicates a lack of systematic error in the slopes of the flux curves chosen for the standards and for the sun.

It can be seen that all four curves are qualitatively similar in overall shape. J1's curve has, however, a much steeper slope in the blue than the other curves. J1's curve also shows a broad spectral dip between 0.5μ and 0.6μ which is not apparent in the other curves. (Note that the UBV measurements lack the spectral resolution necessary to detect this feature.) The quantitative differences in the curves show up clearly in ratios of one curve to another. Figure 8 shows several such ratio curves. From this figure, the steep blue slope of J1 and the presence of the spectral feature in its curve, as well as the comparative similarity of the curves of J2, J3 and J4 are apparent. For J1/J4 and J2/J3 direct ratio data are plotted as open circles.

Changes in Spectral Reflectivity with Orbital Phase. The UBV results given in Harris' article show that the satellites all vary in brightness with orbital phase angle and that the color of J1, J2 and J3 varies to a greater or lesser extent, with J1 having the largest variation. The color variation may be examined in detail by looking at the normalized spectral reflectivity curves at different orbital phase angles. The orbital variation in brightness is given by the variation in the ratio of the satellite to o Virgo at 0.56μ, after the solar phase angle effect has been removed. This section describes the spectrally dependent variation

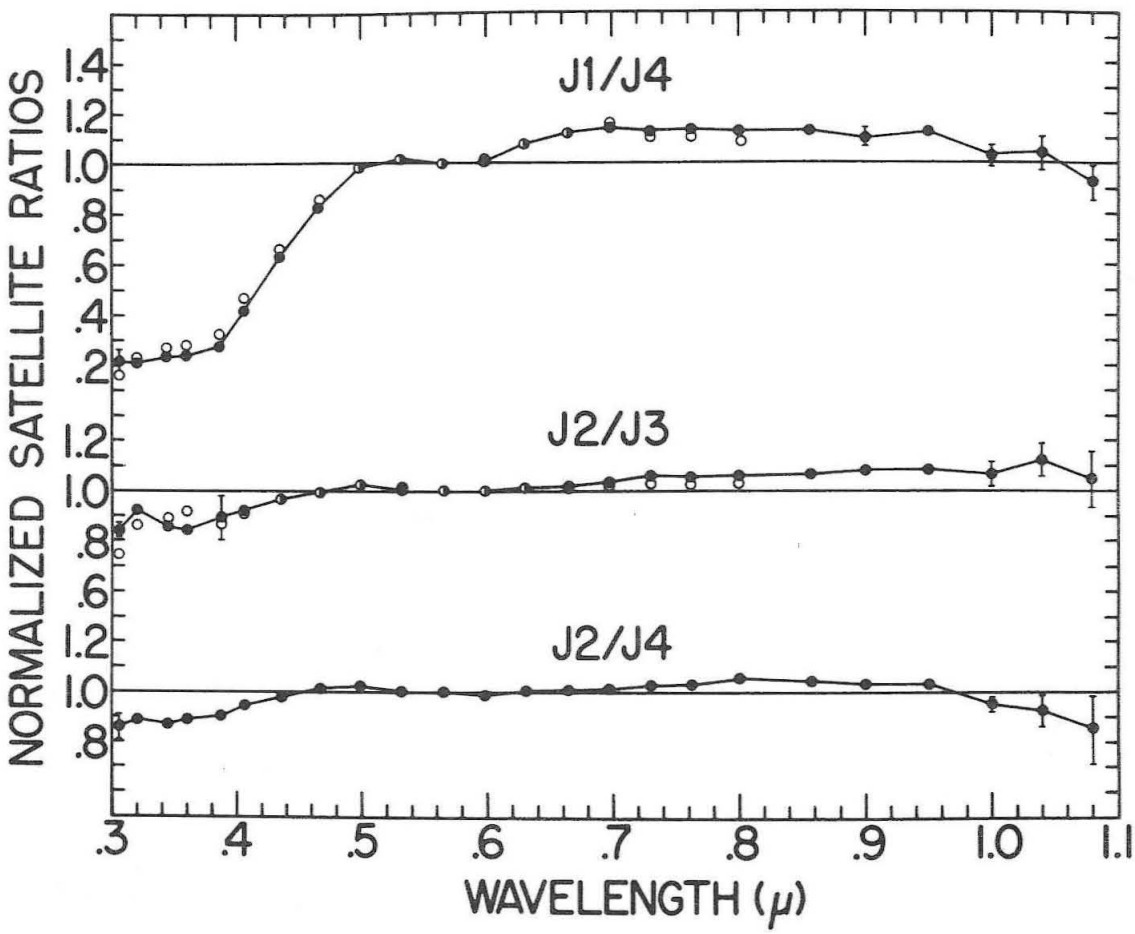

Figure 8. Ratios of the spectral reflectivity curves of several of the satellites.

and the next will deal with the variation in brightness.

Two effective ways to display the variation in spectral reflectivity are, first, to examine the change with orbital phase of the normalized reflectivity at a few selected wavelengths. (Note that since the spectral reflectivity is normalized to $\lambda_0 = 0.56\mu$, the reflectivity at any other wavelength is the ratio of the reflectivity at that wavelength to that at 0.56μ, and therefore, is directly related to the "color difference" in magnitude units by: $m(\lambda) - m(\lambda_0) = -2.5 \log R(\lambda)$.) The second method is to look at the spectral curves at two values of orbital phase angle and at the ratio of these curves.

Figures 9-12 show the variation of the the reflectivity at 0.4μ and 0.72μ as a function of orbital phase angle for each satellite. These values are taken from the reflectivities in the 0.4032μ, 0.406μ filters and the 0.72μ, 0.73μ filters, depending on which filter set was used. The slight difference in effective wavelengths between the filter sets had a negligible effect at 0.72μ because of the relative flatness of the spectral curve in that region; however, the steeper slope of the spectral curve in the blue did produce some difference in the 0.4μ filters. This was corrected for by finding the factor which made the two values agree for J3's curve (which showed little or no variation with orbital phase at this wavelength); this factor was found to be 1.07 and brought the values at all θ's into very good agreement for each satellite.

For J1 (see Fig. 9) the change in the 0.4μ reflectivity is quite large, as expected from the B-V and U-B color variations. The change from maximum to minimum reflectivity at this wavelength corresponds to a color difference of ~0.33 mag., which is between the 0.18 mag. B-V and 0.5 mag. U-B color differences given by Harris. The plot of the 0.72μ reflectivity vs θ also shows a variation, in the opposite sense to the blue variation. This is the first time this

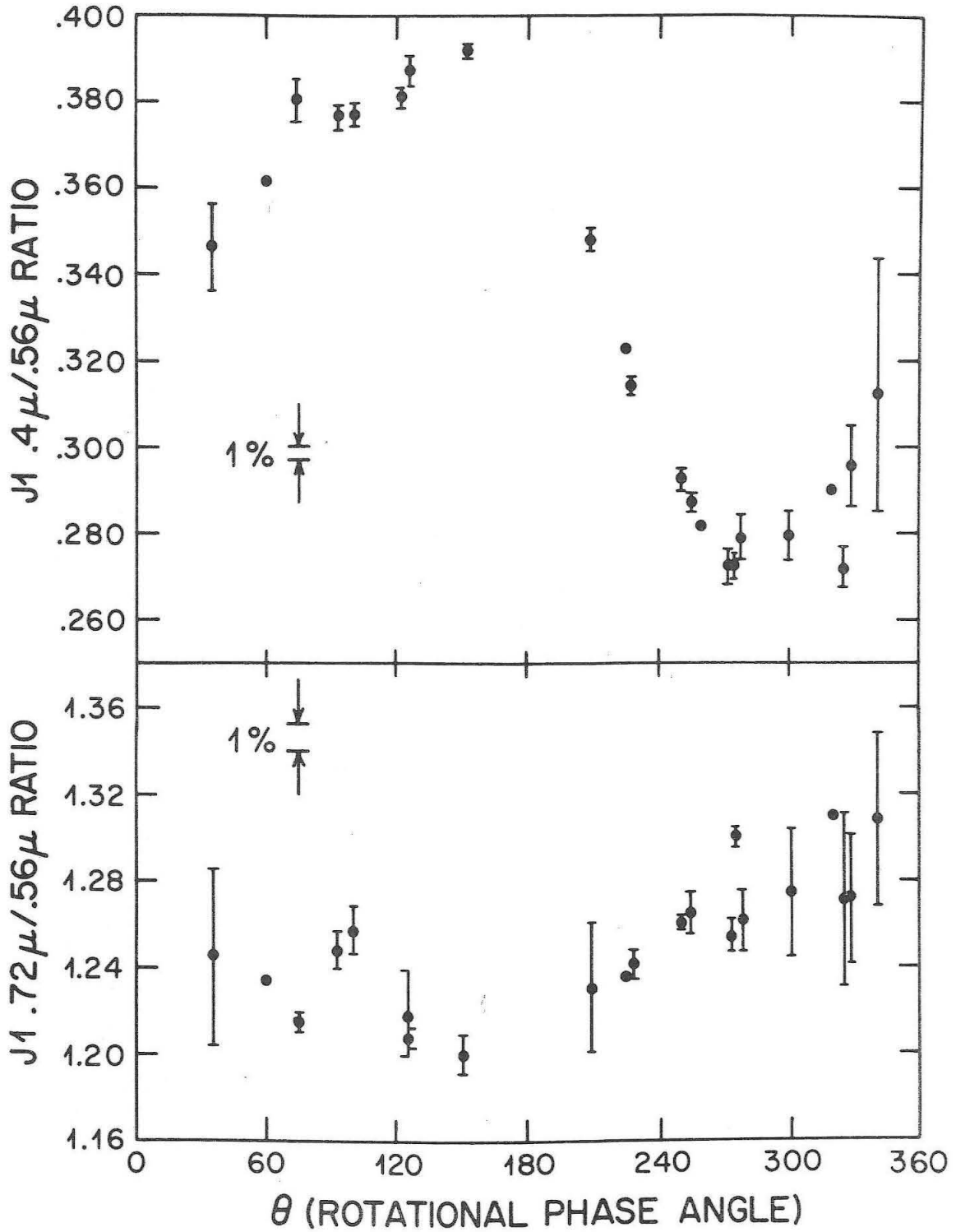

Figure 9. J1 0.72μ/0.56μ ratio; J1 0.4μ/0.56μ ratio.

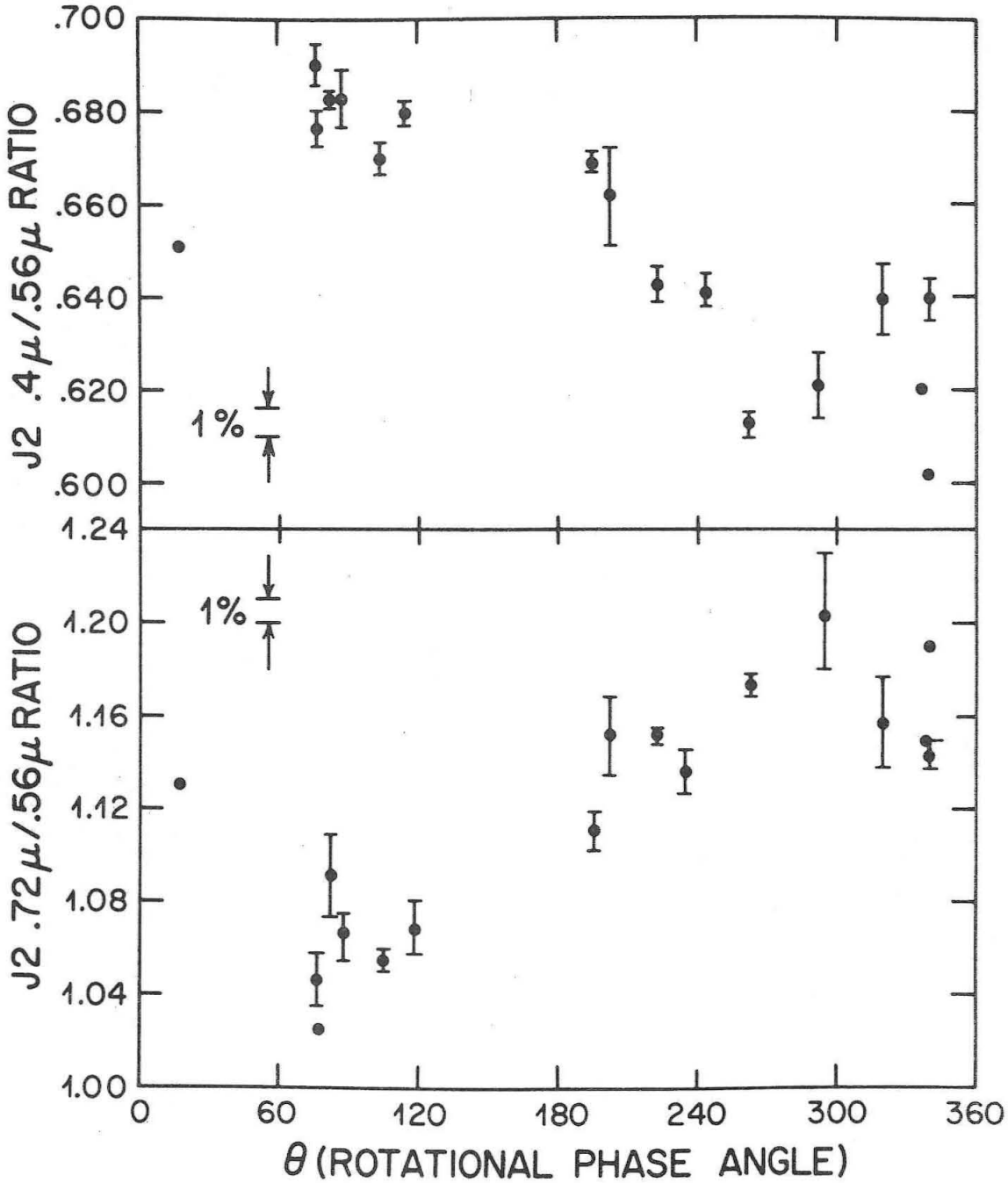

Figure 10. J2 0.72μ/0.56μ ratio; J2 0.4μ/0.56μ ratio.

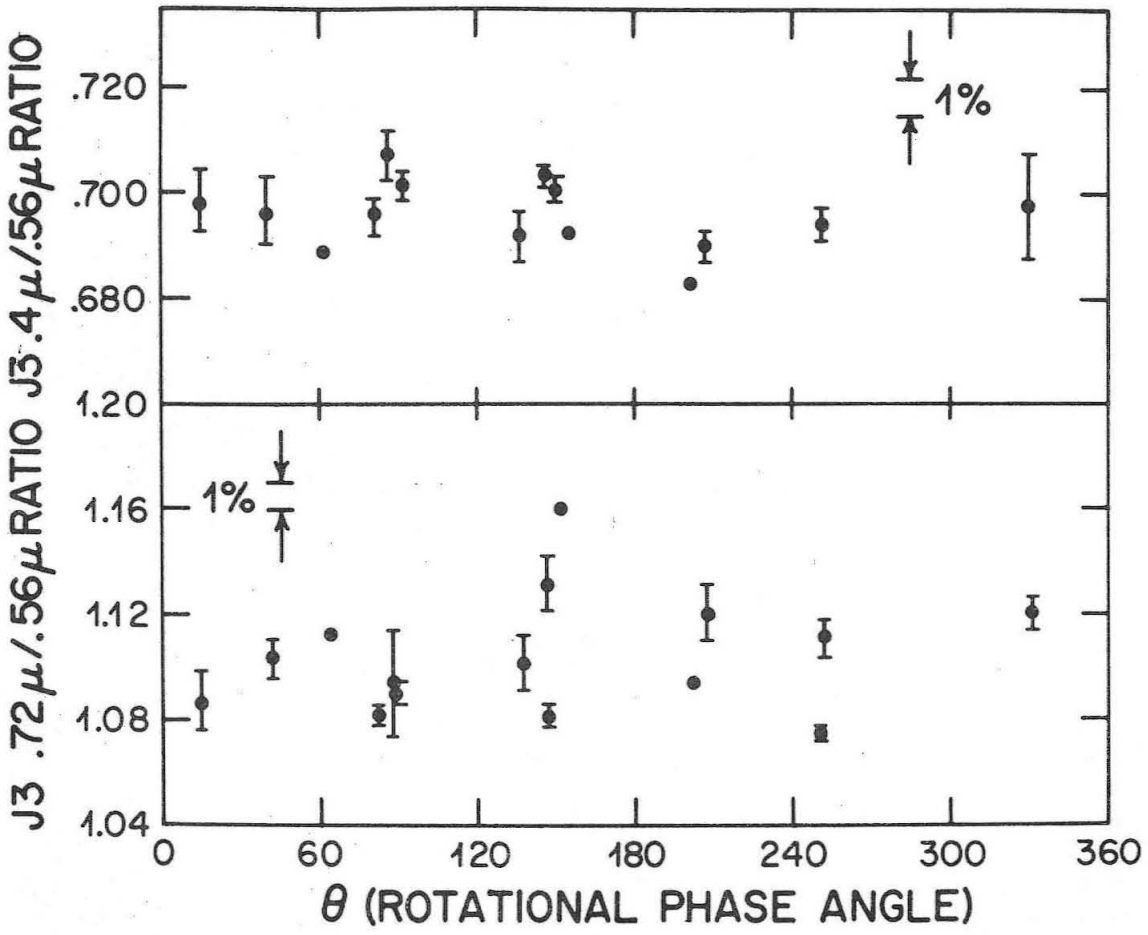

Figure 11. J3 0.72μ/0.56μ ratio; J3 0.4μ/0.56μ ratio.

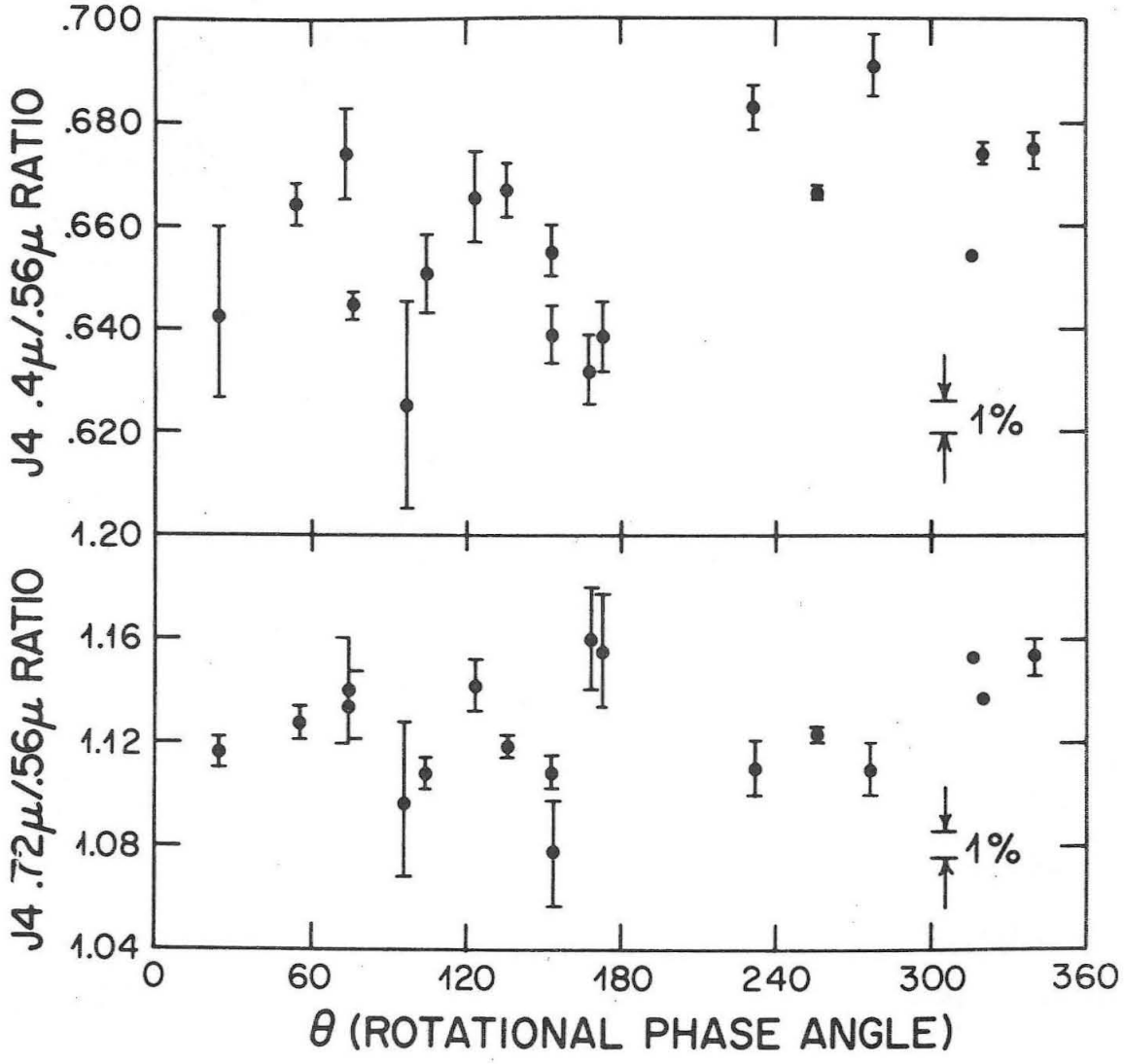

Figure 12. J4 0.72μ/0.56μ ratio; J4 0.4μ/0.56μ ratio.

effect has been noted (to the author's knowledge); Harris gives reflectivities for the R(λ_{eff} = 0.690) and I(λ_{eff} = 0.820) filters but mentions no variation in R-V or I-V color with θ.

J2 (Fig. 10)exhibits a much smaller change in 0.4μ reflectivity; again, this is consistent with the UBV data which indicates no change in B-V color but shows evidence for ~0.2 mag. difference in U-B color. A variation in 0.72μ reflectivity is evident here also; again, no previous mention of such an orbital phase effect at this wavelength is known.

J3(Fig. 11) shows no appreciable effect at either 0.4μ or 0.72μ. Harris indicates the probability of a U-B color change of 0.04 mag.; and, as will be shown shortly, a variation with θ for wavelengths shorter than 0.4μ was noted in the UV-Vis measurements made in this study.

Although the scatter is slightly greater, J4 (Fig. 12) shows a change in 0.4μ reflectivity with θ of slightly smaller magnitude than that shown by J2 but in the opposite sense, the trailing side having a slightly higher 0.4μ reflectivity. No significant change in 0.72μ was noted. Harris lists no variation at all in U-B or B-V color for this satellite.

It should be noted that these curves contain points taken over the entire range of solar phase angle, α, covered (0 to ~9 deg). The smoothness of the curves indicates, therefore, that there is no α-dependent spectral effect present of the same magnitude as the orbital phase effect. There may be a small effect due to α in J4's 0.4μ and 0.72μ curves, but this is based primarily on the relatively greater scatter of the points compared to the other satellites and is not conclusive.

In order to illustrate the variation in spectral reflectivity over the range 0.3μ to 1.1μ between two values of θ, the ratio of the spectral curve at θ_1 is

taken with respect to the spectral curve at θ_2. Figure 13 shows such a ratio as a function of wavelength for each satellite. These ratios are the ratios of composite curves for θ>180 deg (trailing side) to θ<180 deg (leading side) in each case. Because of the lack of complete phase coverage in the UV-Vis and Vis-IR mentioned earlier, the composite curves ratioed here are not always taken at the extrema of the spectral variations illustrated in Figs. 9-12. Table 5 gives the date, number of observations, and θ's for each of the curves used in the composites.

The ratio curve for J1 shows that the variation noted in the 0.4μ filters (Fig. 9) is part of a systematic change extending from 0.3μ to 0.5μ. The open circles represent the maximum changes in the U and B filters (Harris, 1961). The discrepancy between the U filter point and the ultraviolet points from this study is probably due to the J1 composite curves not being taken at the extrema of the spectral change. Also, the leading side UV-Vis data was obtained through a secondary reduction from a J1/J4 direct ratio and the J4 composite curve. The error in this double reduction may account for the high 0.3μ ratio, or this feature may be real. The 0.72μ effect noted in the discussion of Fig. 9 is evident here, although the magnitude is reduced due to using composite curves. This effect seems to be part of a larger spectral variation extending from ~0.68μ to ~0.9μ.

J2's ratio curve shows an ultraviolet feature similar in form to that of J1 but of less depth and extending only just beyond 0.4μ (the small but detectable variation at 0.4μ is shown in Fig. 10). The approximately 20% variation in the U filter and the lack of variation in the V filter reported by Harris (plotted as open circles) are in agreement with the feature observed here. The 0.72μ variation plotted in Fig. 10 can be seen from Fig. 13 to be part of a broader spectral feature similar to J1's 0.72μ variation, although the full magnitude of the effect

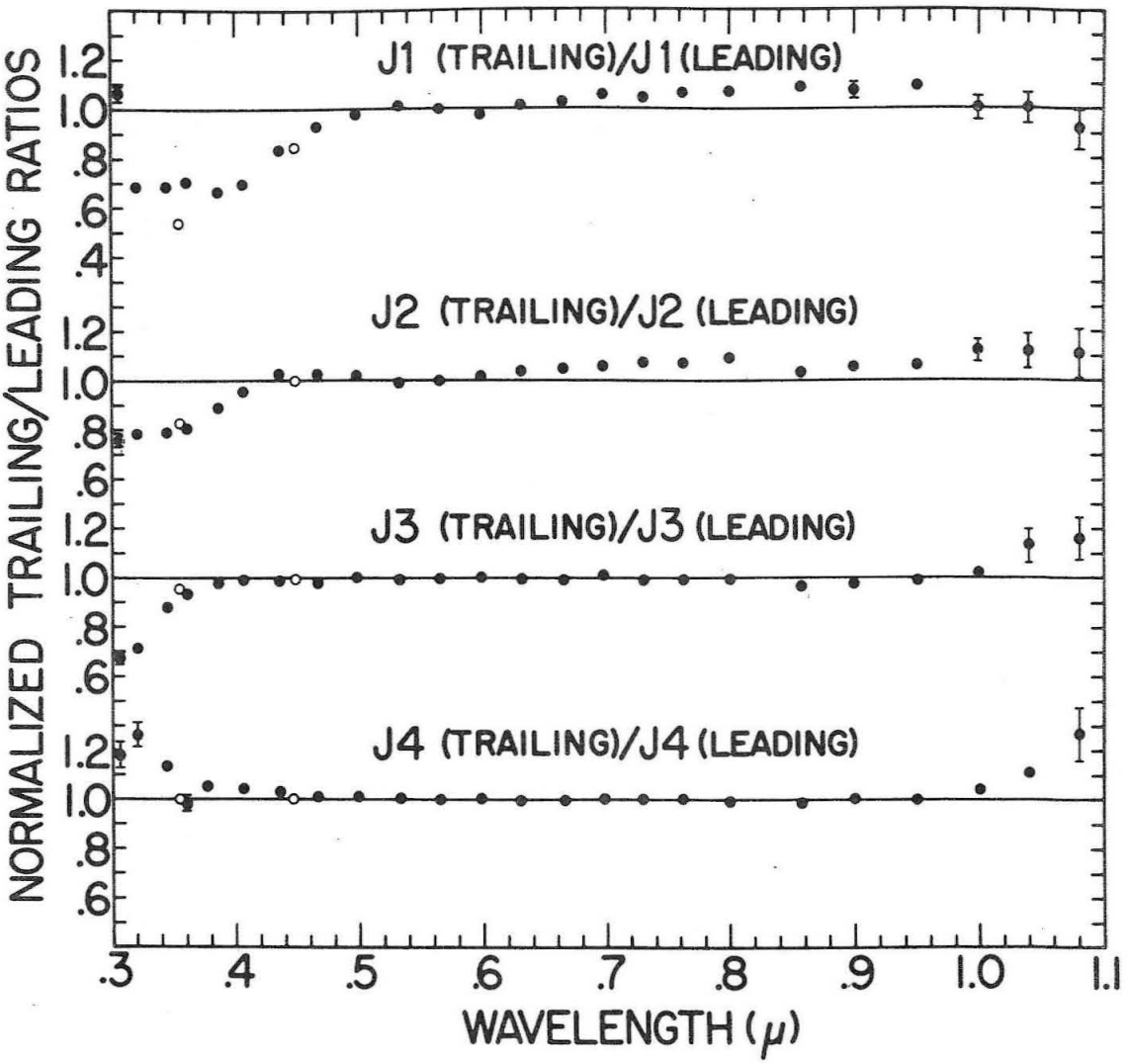

Figure 13. Ratio of the spectral reflectivity for θ>180 deg (trailing side) to that for θ<180 deg (leading side) for each satellite.

Table 5. Composite Curves for Trailing and Leading Sides

Satellite	Trailing Side (θ >180 deg) Date	Filter Set	θ (deg)	Number of Observations	Leading Side (θ<180 deg) Date	Filter Set	θ (deg)	Number of Observations
J1	04/18/69	UV-Vis	273	5	04/17/69 (relative to J4)	UV-Vis	60	3
	04/13/69	Vis-IR	325	3	04/17/69	Vis-IR	75	2
	04/20/69	Vis-IR	328	2	04/21/69	Vis-IR	152	2
	04/22/69	Vis-IR	340	2	05/12/69	Vis-IR	100	4
	05/13/69	Vis-IR	300	3				
J2	04/16/69	UV-Vis	235	5	04/29/69	UV-Vis	105	6
	04/13/69	Vis-IR	295	2	04/21/69	Vis-IR	19	1
	04/17/69	Vis-IR	339	1	05/13/69	Vis-IR	79	1
	05/12/69	Vis-IR	340	1				
J3	04/18/69	UV-Vis	250	2	04/16/69	UV-Vis	148	6
	04/17/69	Vis-IR	202	1	04/22/69	UV-Vis	90	2
					04/29/69	UV-Vis	82	7
					04/21/69	Vis-IR	41	3
					05/12/69	Vis-IR	151	1
					05/13/69	Vis-IR	63	1
J4	04/16/69	UV-Vis	232	6	04/29/69	UV-Vis	154	9
	04/18/69	UV-Vis	277	5	04/13/69	Vis-IR	168	4
	04/17/69	Vis-IR	256	2	05/12/69	Vis-IR	75	3
	04/20/69	Vis-IR	316	1	05/13/69	Vis-IR	96	3
	04/21/69	Vis-IR	340	3				

is again not evident because curves at several θ's were averaged to produce the composite curves.

The ultraviolet feature in J3's ratio curve does not appear until ~0.38μ. The shape of the feature from 0.3μ to 0.38μ is similar to the steep slopes of J1's and J2's features, but it cannot be determined here whether the feature levels off below 0.3μ, as would be expected if the feature is qualitatively like those of J1's and J2's curves. The evidence for this feature is weaker than for those in J1 and J2, since it is based on only two samples of the trailing side in the UV-Vis filters, and since there is no variation evident in the Vis part of the spectrum. The slight effect in the U filter reported by Harris (open circles) is supporting evidence for the existence of this feature. No significant feature in the spectral range of the 0.72μ features in J1 and J2's curves can be seen, confirming the flat 0.72μ curve shown in Fig. 11. The slightly high values of the 1.04μ and 1.08μ ratios must be regarded as very inconclusive since these points are based on only one observation of the trailing side with the Vis-IR filters.

The ratio curve for J4 shows an ultraviolet feature somewhat similar in shape to the ones described above, but in the opposite sense to that of the other satellites, that is, the trailing side has a somewhat higher ultraviolet normalized reflectivity than the leading side. This is in agreement with Fig. 12, which indicates a 0.4μ reflectivity for the leading side slightly lower than that of the trailing side. Since the overall change in the ultraviolet is similar in magnitude to that of J3, it might be possible to observe this change with the U filter. Harris reports no such variation; this may be due to the smaller effect at 0.3μ and 0.32μ(~20% for J4, as opposed to ~30% for J3), since the U filter integrates flux over a large spectral bandpass. No effect in the region of 0.72μ can be seen, but the slight rise of the curve from 1.0μ to 1.1μ may be real since it is

based on 6-10 observations of both sides in the Vis-IR filters.

Brightness Variations with Solar Phase Angle and Orbital Phase. Since the brightness change due to solar phase angle over the period of a satellite may be of the same order as the variation due to θ, the two effects are difficult to separate. Stebbins (1926) first determined the phase functions of the satellites photoelectrically by assuming a phase law in the form of Equation 15, choosing the first and second degree coefficients until the brightness vs θ curve was smooth. Harris used the phase functions so derived by Stebbins to reduce most of the Mt. Hamilton observations given in his article.

The method adopted here is a modification of the above. The quantity given in Equation 18 was plotted against θ for different choices of $\phi(\alpha)$:

18). $$K(\lambda_0,\theta) = \left[\frac{f_{\text{satellite}}(\lambda_0,\theta)}{f_{\text{o Virgo}}(\lambda_0)}\right]\left[\frac{r\Delta}{a(a-1)}\right]^2\left[\phi^{-1}(\alpha)\right]$$

r = sun-planet distance in AU

Δ = earth-planet distance in AU

a = semimajor axis of Jupiter = 5.2028 AU

$\phi(\alpha) = 10^{-0.4(A\alpha + B\alpha^2)}$

$K(\lambda_0,\theta)$ is related directly to the mean opposition magnitudes of the satellites by:

19). $$\overline{m}_{\text{satellite}}(\lambda_0,\theta) - m_{\text{o Virgo}}(\lambda_0) = -2.5 \log K(\lambda_0,\theta)$$

and to $p(\lambda_0)$, from Equation 13, by:

20). $$p_{\text{satellite}}(\lambda_0) = \left[\frac{K(\lambda_0,\theta)}{R^2}\right]\left[a(a-1)\right]^2\left[\frac{f_{\text{o Virgo}}(\lambda_0)}{f_{\alpha\ \text{Leo}}(\lambda_0)}\right]\left[\frac{F_{\alpha\ \text{Leo}}(\lambda_0)}{F_{\odot}(\lambda_0)}\right]$$

Stebbins' phase coefficients A and B were used as first approximations in the calculation of $\phi(\alpha)$. The resulting curves of $K(\lambda_0,\theta)$ vs orbital phase were relatively smooth. Small variations of A improved the orbital phase curves in some cases,

however. The sensitivity of this type of determination is not extremely high, especially as few observations immediately before or after opposition were obtained. Figures 14-17 illustrate the change in orbital phase variation as A is varied approximately 20-30% around the value chosen as best for each satellite. The error bars represent the standard deviation of the average value of the satellite vs star ratios and do not indicate the errors in the choice of phase law. Points without error bars have errors less than or equal to the diameter of the point. Points plotted as x's represent values for single observations and should not be given the same weight as the average points.

The central curve in each figure is the curve resulting from the A coefficient chosen as best. Each point is labeled with the phase angle at which it was taken. One of the major criteria used to choose the best A value and the limits of variation was the separation of points taken at nearly the same θ but at different α's. It can be seen in these figures that as A is varied in either direction from the chosen value, such points separate, points with larger α's moving down relatively with decreasing A and up with increasing A. The best value of A was chosen to minimize scatter in this sense.

Several points should be mentioned here. The scatter, even for the A's chosen, is on the order of several percent. This may be due to the form of the phase law not being exactly right; the moon shows an "opposition" effect very close to $\alpha = 0$ deg which is not taken into account by Equation 15 (Van Diggelen, 1965). Also, variation of the second coefficient, B, was not considered, because of the lack of observations near opposition. Several anomalous points, such as the low point at 300 deg in J1's curve and the high point at 252 deg in J3's curve, are averages of only two or three observations. Scatter in J4's curve may be a result of different phase laws for different θ's as indicated by Harris (1961).

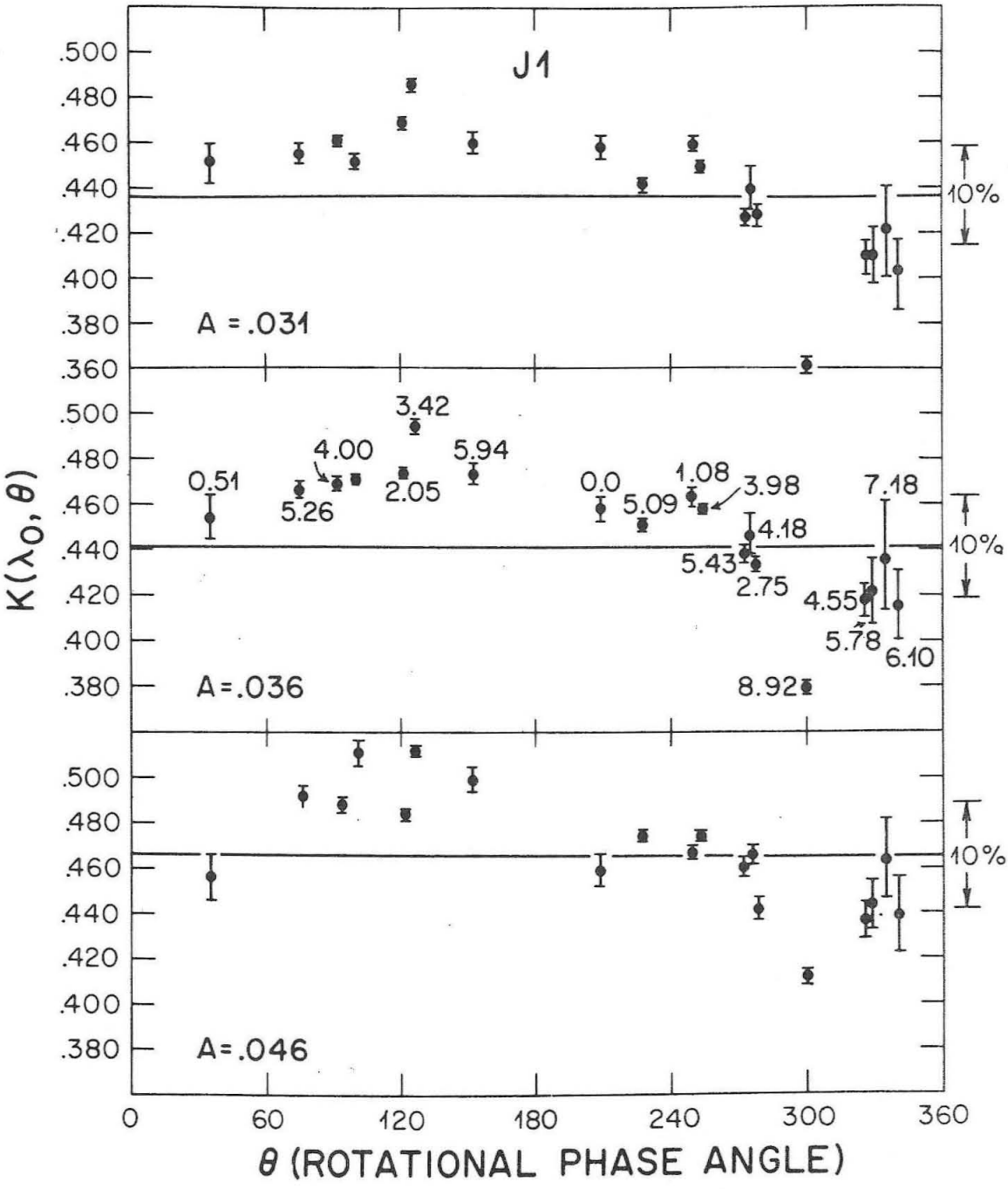

Figure 14. $K(\lambda_0,\theta)$, the ratio of the flux of the satellite to that of o Virgo at λ_0 and mean opposition as a function of θ for three choices of the phase coefficient, A. The center value was chosen as the best value of A. The α value for each data point is shown in the center graph.

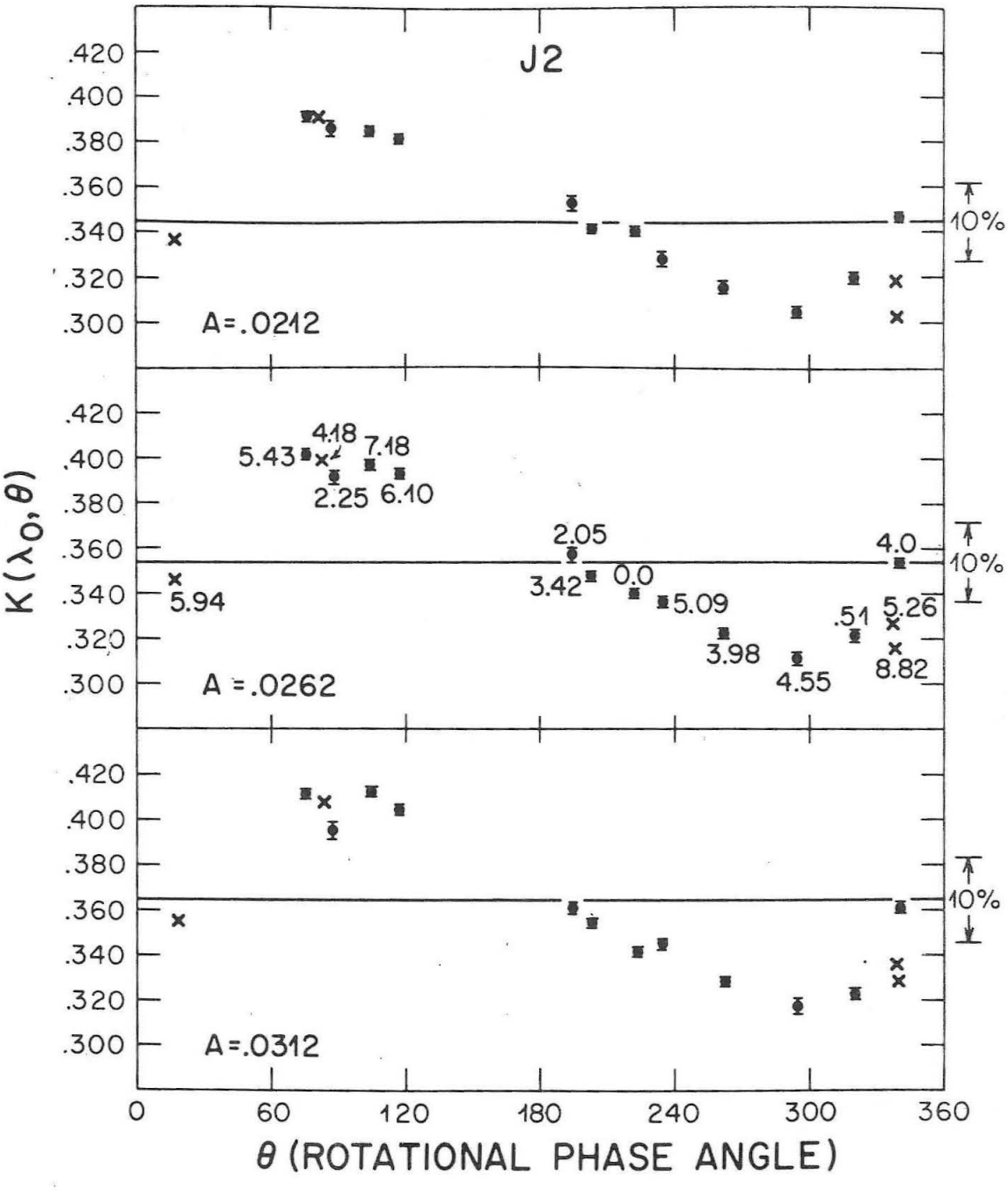

Figure 15. $K(\lambda_0,\theta)$, the ratio of the flux of the satellite to that of o Virgo at λ_0 and mean opposition as a function of θ for three choices of the phase coefficient, A. The center value was chosen as the best value of A. The α value for each data point is shown in the center graph.

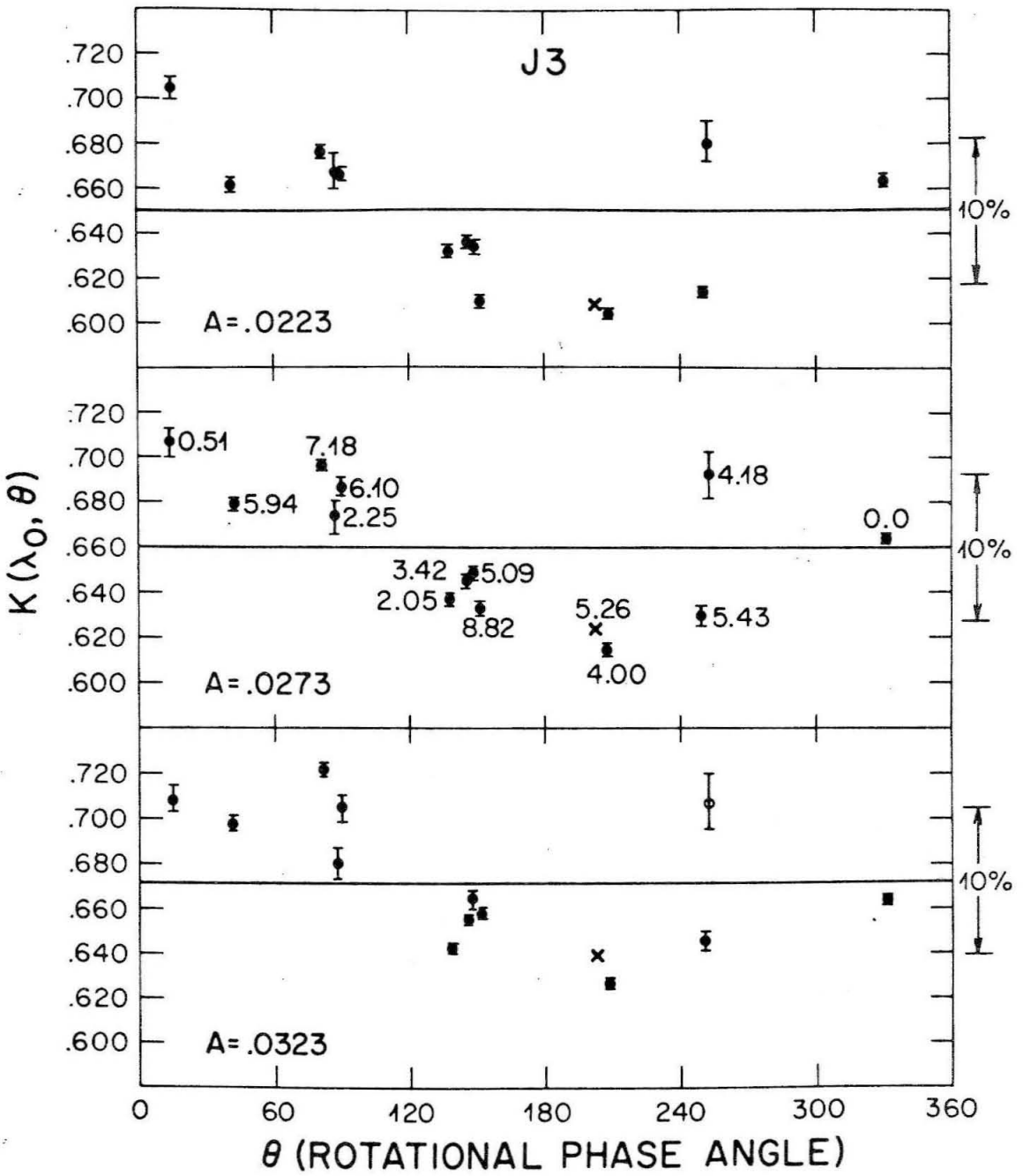

Figure 16. $K(\lambda_0,\theta)$, the ratio of the flux of the satellite to that of o Virgo at λ_0 and mean opposition, as a function of θ for three choices of the phase coefficient, A. The center value was chosen as the best value of a. The α value for each data point is shown in the center graph.

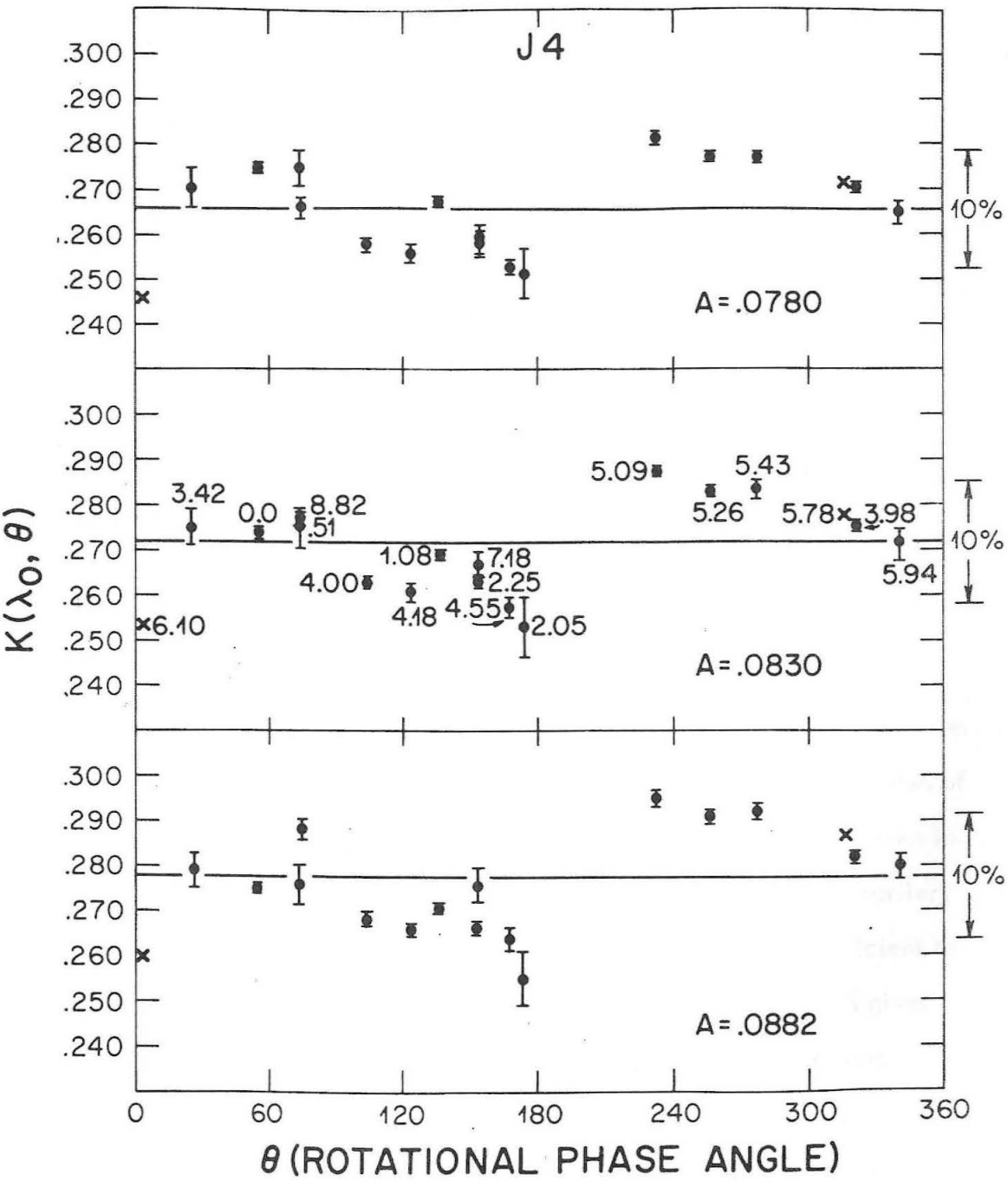

Figure 17. $K(\lambda_0,\theta)$, the ratio of the flux of the satellite to that of o Virgo at λ_0 and mean opposition, as a function of θ for three choices of the phase coefficient, A. The center value was chosen as the best value of A. The α value for each data point is shown in the center graph.

Not enough data near opposition were taken in this study to definitely confirm this effect. Finally, the variation of A, as shown, does not affect the mean value of $K(\lambda_0,\theta)$ by more than a few percent. Thus, the major uncertainty in the brightness of the satellites comes from the uncertainty in the limits of the rotational variation. Table 6 lists Stebbins' values of A and B and the value chosen from this study for each of the satellites. Note that the largest difference is for J1; this is not unreasonable when one considers that the errors in Stebbins' early observations are probably greatest for observations near the planet due to scattered light.

Table 6. Phase Law Coefficients

Satellite	A(Stebbins)	A(Best Fit)	B(Stebbins)
J1	0.0460	0.0360	-0.00100
J2	0.0312	0.0262	-0.00125
J3	0.0323	0.0273	-0.00066
J4	0.0780	0.0830	-0.00270

Figure 18 shows the phase law, $\phi(\alpha)$, (0-10 deg), for each of the satellites, calculated from the coefficients in Table 6. Also included are the phase laws of the moon and Mercury taken from Harris (1961). The moon's phase law given in Harris does not include the "flash up" or "opposition effect" mentioned earlier, but since the near opposition observations of the satellites were not sufficient to see such an effect in their phase laws, the average $\phi(\alpha)$ given by Harris gives some indication of how the satellites compare with the moon over the range of 0-10 deg.

Table 7 gives the mean value of $K(\lambda_0,\theta)$, $\overline{K(\lambda_0)}$, for each of the satellites, the mean opposition magnitude which corresponds to $\overline{K(\lambda_0)}$, and the maximum variation due to orbital phase angle. It also contains the mean opposition magnitudes in the V filter and rotational variation from Harris' article.

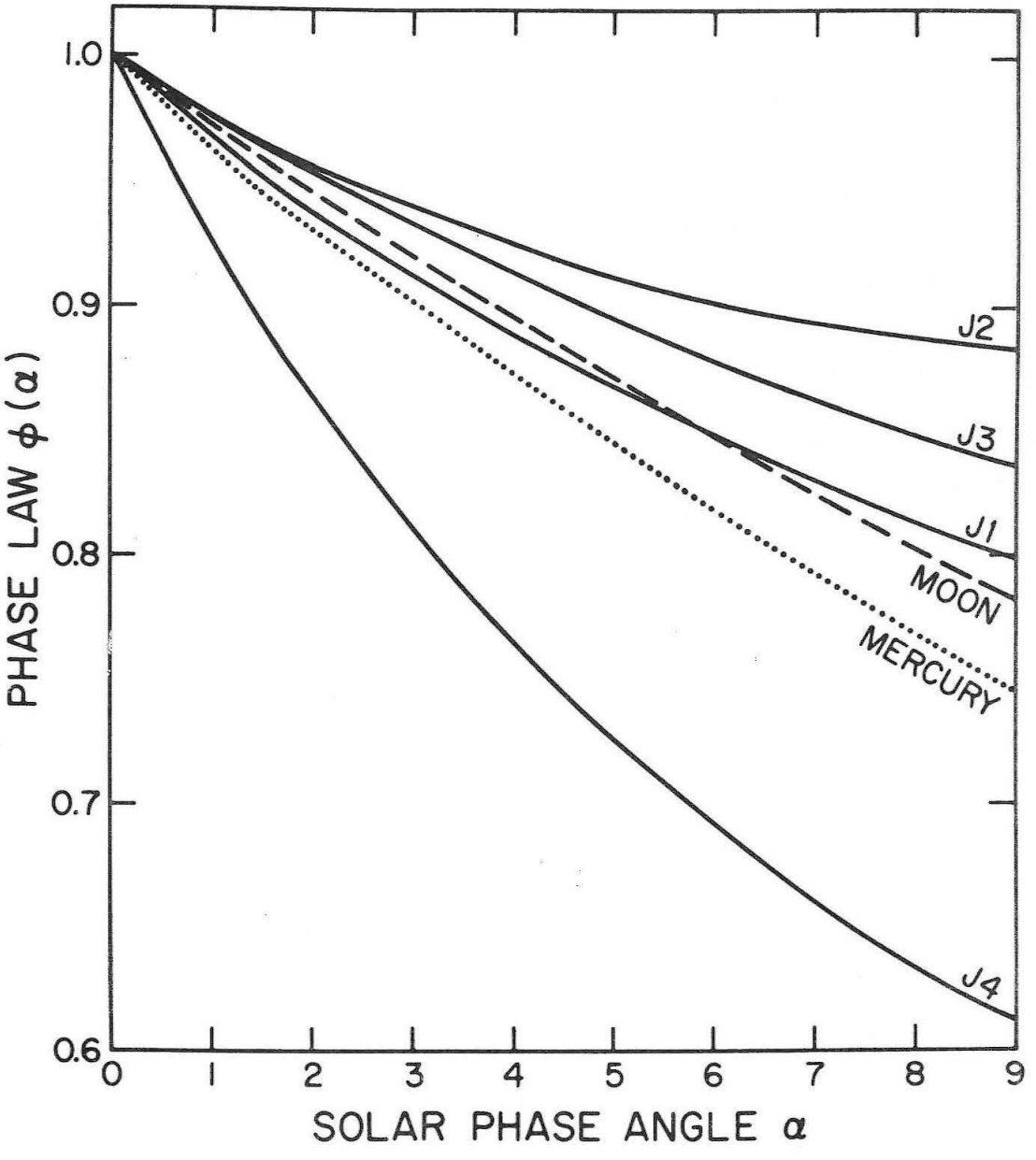

Figure 18. The phase law, $\phi(\alpha)$, for the four Galilean satellites, the moon and Mercury over the first 10 deg of the solar phase angle.

Table 7. Mean Opposition Magnitudes

Satellite	$\overline{K(\lambda_0)}$	This Study $\overline{m}_0$ (mag.)	This Study Maximum Rotational Variation (mag.)	Harris $\overline{m}_0$ (mag.)	Harris Maximum Rotational Variation (mag.)
J1	0.442	4.88	0.22	4.80	0.21
J2	0.354	5.13	0.28	5.17	0.34
J3	0.660	4.44	0.14	4.54	0.16
J4	0.272	5.41	0.14	5.50	0.16 (for $\alpha>8$ deg)

Geometric Albedo and Density. In order to determine the Bond albedo, both the geometric albedo and the phase integral must be known. The geometric albedos of the satellites will be discussed in this section, and the Bond albedo and phase integral (which must be estimated since $\phi(\alpha)$ is known only over a small range of α) will be discussed in the next section.

Equation 20 gives $p(\lambda_0)$ in terms of measured or calculated quantities. The only quantity in this expression which has not been discussed yet is the satellite radius, R. As mentioned before, the radii of these objects are difficult to measure due to the small disk they present.

A good review of the available methods for measuring planetary diameters and a discussion of the errors involved with each method is given in Sharonov (1958) along with the most important observations of the diameters of many bodies in the solar system, including the Galilean satellites. Table 8, taken from Sharonov, gives diameters measured for the Galilean satellites; the following paragraphs give a brief description of each method and a comment on the types of errors possible, also following Sharonov.

Table 8. Diameters of the Galilean Satellites

Observer	Method of Measurement	Angular Diameter 5 AU J1	J2	J3	J4
1. Sallet and Bosler	Double Image Micrometer	0".98	0".91	1".43	1".33
2. Michelson	Interferometer	0".95	0".88	1".25	1".21
3. Hamy	Interferometer	0".86	0".78	1".14	1".15
4. Danjon	Interferometer	0".90	0".78	1".22	1".08
5. Camichel	Discometer	0".90	0".78	1".35	1".26
6. Dollfus	Double Image Micrometer	0".97	0".85	1".38	1".52
7. Mean		0".93	0".83	1".29	1".26

Measurements with the double image micrometer are made by bringing two images produced by a birefringent polarizing prism into contact. Sharonov regards this as having the highest accuracy of the standard methods although it still suffers from effects which blur the edge of the object, such as seeing, focus inaccuracies and irradiation (the physiological effect that tends to make bright objects look larger).

The Discometer, developed by Camichel, produces an "artificial planet" of the same color and brightness next to the real object by optical means. The size is then adjusted to match the object and the images superimposed. The superposition is done from both the right and left and the mean taken to cancel systematic effects. The method has the advantage that accidental errors are the same for both large and small disks. The accuracy of the method is limited by image shimmering, limb darkening, and dark markings on the object measured. Although the accidental error for one measurement is quite small, readings taken at Pic du Midi on different evenings have a scatter of 5-10% (Sharonov, 1958).

Sharonov regards the knowledge of systematic errors in this system as incomplete.

Interferometric measurements, where available, should have accuracies as high or higher than the above methods. Interferometry, developed by Michelson (1891), consists of observing the fringe visibility function of the object, particularly the zeros of visibility function. From this, the angular size of the object can be determined.

Measurements of the radii of the satellites also affect another important parameter, the satellites' densities, ρ. The masses of the satellites can be determined from the mutual perturbations in their orbits. Two solutions to this problem are commonly quoted, that of Sampson and that of De Sitter. Table 9 gives the masses of the satellites from each of these sources (Porter, 1960).

Table 9. Satellite Masses

	Mass ($\times 10^{24}$ gm)	
Satellite	De Sitter	Sampson
J1	73	86.5
J2	47.5	56.3
J3	154.0	182.5
J4	95.0	112.6

To illustrate the manner in which $p(\lambda_0)$ and ρ depend on the radii chosen, Fig. 19 shows, for each satellite, a region in the p-ρ plane and a point which represents the $p(\lambda_0)$ and ρ for the mean diameter in Table 8. The horizontal error bar on the mean point gives the limits of the two sets of mass determinations in Table 9. The vertical error bar represents the limit of rotational variation. The region shown for each satellite is the area swept out by the error bars as the diameter is varied through the values in Table 8. The possible ± 0.1 mag. error in $m_\odot$ will affect these regions by moving each mean point up or down by ~10%. These

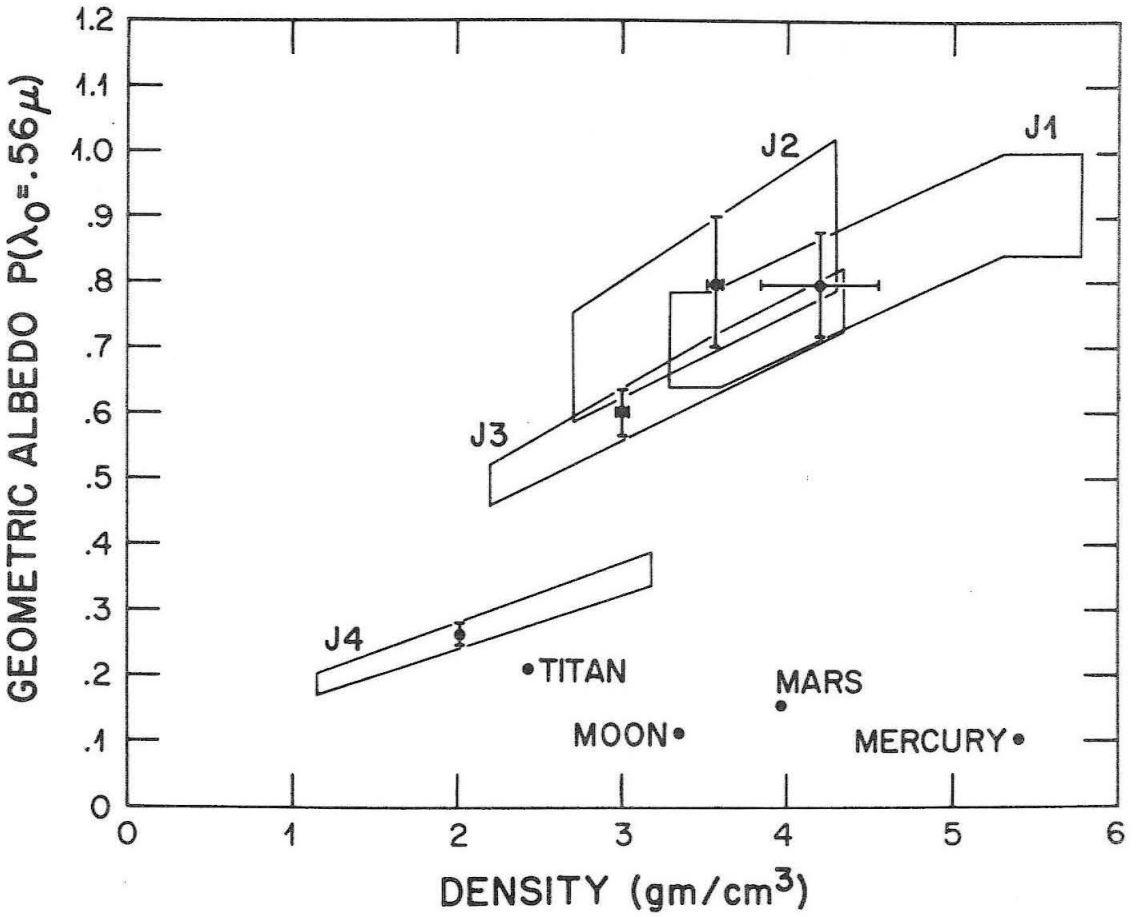

Figure 19. Geometric albedo vs density of the satellites. The point for each satellite represents the values of p and ρ for the mean of the measured diameters. The density error bar gives the limits of two mass determinations (Porter, 1960) and the geometric albedo range is determined from the rotation variation shown by the satellite. The regions indicated for each satellite indicate the limits of the given error bars for the range of diameter measurements compiled by Sharonov (1958).

regions thus represent the ranges of p, ρ values possible within the given errors for the satellites. The values of p and ρ for Mercury, the moon, Mars and Titan are shown for reference.

By comparing the diameters of Table 8 with the method of determining these diameters, it seems that the interferometric measurements tend to yield smaller diameters and therefore higher albedos than the micrometer measurements, with the Discometer results somewhere in between. This indicates systematic errors in the methods used, and makes the evaluation of a "best" value for p and ρ difficult. The mean values of the satellite diameters given by Sharonov have been used to determine the value of p for each satellite given in Table 10, but it should be remembered that a value anywhere in the regions outlined above is probably as likely, and indeed these values, especially for the two smaller satellites, may be off by considerably more.

Table 10. Mean Geometric Albedos

Satellite	Albedo
J1	0.792
J2	0.796
J3	0.615
J4	0.266

Even within the above limits, several general observations can be made. While J1, J2 and J3 have high geometric albedos, above 0.5 or 0.6, and have densities above ~3 gm/cm^3, J4 has a distinctly lower geometric albedo and density than the other satellites. Also, despite the large errors due to uncertainties in radii, all of the satellites have p and ρ regions far different from Mercury, the moon, or Mars, and only J4 approaches the p and ρ values of Titan, whose radius is also uncertain due to its small apparent size.

Bond Albedo and Phase Integral. In order to find the Bond albedo of a satellite, the phase integral, q, must be known. The Bond albedo is a more physically meaningful quantity than the geometric albedo since it represents the ratio of incoming energy to outgoing energy for a surface. Unfortunately, because of the limited range of phase angle over which Jupiter can be observed (0 to ~12 deg), the phase integral is not known very accurately. Two methods that have been used to estimate q are: first, to assume that the surface is lunar-like and use the q for the moon; and second, to adopt some empirical or semi-empirical law relating the phase coefficient to the phase integral.

The first procedure is the one adopted by Harris. The arguments for this method are: first, that both the moon and Mercury have nearly the same q, despite very different environments; and second, it has been noted in laboratory studies, (Hapke, 1963) that the composition of the surface does not strongly affect q as long as the necessary surface macrostructure is present and the materials are of low albedo.

On the other side, there is the fact that the satellites show variety in their phase functions over the first 10 deg. Figure 18 shows the phase functions, $\phi(\alpha)$, for the satellites as well as for the moon and Mercury. It can be seen that, over the first 10 deg of α at least, J1 is similar to the moon, J4 is more backscattering, and J2 and J3 are less backscattering than the moon. Since the largest contributions to the phase integral, q, are made at larger angles than 10 deg, this initial behavior of $\phi(\alpha)$ cannot be regarded as conclusive. It does, however, indicate that the application of the lunar value of q to all of the satellites may not be a good approximation.

Another fact which suggests that the assumption of the lunar q for the satellites is not necessarily good is the great difference between the geometric

albedos of the satellites and that of the moon. As Fig. 19 shows, even J4 has a geometric albedo more than twice that of the moon and J1, J2 and J3 all greatly exceed the moon in geometric albedo. Hapke's work (1963) indicates both experimentally and theoretically that surfaces of high albedo approach the phase law of a Lambert surface, that is, higher values of q. Even the relatively sharp decrease in brightness from 0 deg to 10 deg phase shown by the satellites (Fig. 18) does not rule out high values of q since it has been shown (Oetking, 1966) that even near-Lambert surfaces exhibit an "opposition effect" near zero phase. It is the behavior of the phase law at larger phase angles (usually 30-60 deg) which determines the value of the phase integral.

The adoption of an empirical law is also fraught with problems. Several schemes have been proposed, the best known probably being Russell's Law, which states that $q = 2.2\,\phi(50 \text{ deg})$. This law yields very good results for a surprising variety of theoretical and observed phase functions (Harris, 1961); however, it requires, for its proper application, knowledge of $\phi(50 \text{ deg})$, which reduces its usefulness for objects with heliocentric distances greater than that of Mars.

An extension of Russell's Law was proposed by Stumpff (1947). Stumpff used the fact that $\phi(50 \text{ deg})$ can be estimated by assuming a linear form of the phase function in magnitude units, $\Delta m(\alpha) \approx A\alpha$. If one uses $\Delta m(\alpha) \approx A\alpha$, $\phi(50 \text{ deg})$ is given by $\exp(20A/\log e)$, and Russell's Law then gives:

21). $\qquad \log q = 0.34242 - 20A$

This function, shown in Fig. 20, agreed quite well with the values of q and A for Venus, Mercury, the moon, and Mars available to Stumpff (plotted as filled circles). However, more modern determinations of these quantities (plotted as

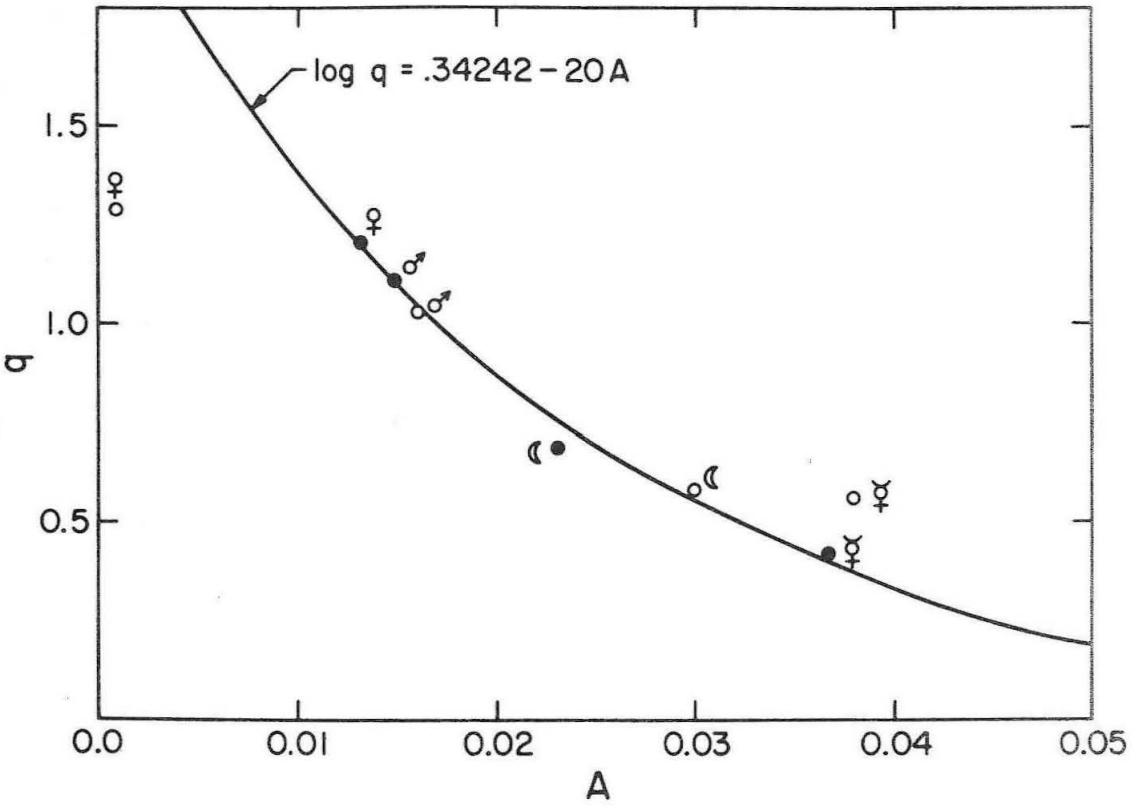

Figure 20. Phase integral, q, vs phase coefficient, A, for several bodies, giving old (filled circles) and new (open circles) values. The curve shown is calculated from the extension of Russell's Law proposed by Stumpff (1948).

open circles) do not fit so well (Harris, 1961; Allen, 1963). The discrepancy at large A arises primarily from the higher q value for Mercury now accepted.

Table 11 gives values of the Bond albedos of the satellites at 0.56μ calculated both with the lunar q and with the q from Stumpff's formula, using the mean value of p found in this study. The differences are large and estimates of the Bond albedo should probably be regarded very critically until better determinations of the radii and phase integrals of the satellites are available.

Table 11. Bond Albedos

	q		A	
Satellite	Lunar	Stumpff	Lunar	Stumpff
J1	0.585	0.420	0.463	0.333
J2	0.585	0.530	0.465	0.422
J3	0.585	0.510	0.359	0.313
J4	0.585	0.048	0.156	0.012

Eclipse Brightening. Binder and Cruikshank have reported that J1 and, to a lesser extent, J2, are anomalously bright for a period of about 15 minutes after emerging from Jupiter's shadow (Binder and Cruikshank, 1964 and 1966a). Although observation of eclipse reappearances was not a major objective of the present observational program, data were obtained on a particularly favorable reappearance of J1 on 1 May 1969.

The observation was carried out with the same equipment as was the rest of the program on the 24-inch telescope. Only two of the filters were used, with effective wavelengths of 0.4350μ and 0.5650μ. The full filter set could not be used because of the short time in which the observations had to be made. The second beam of the photometer was positioned to remove the sky background as soon as J1 could be seen reappearing. Three 5-second integrations were performed with one filter in place, then the other filter was placed behind the

aperture and three more integrations taken. This procedure was continued for about 40 minutes after J1 was first seen. Observations of J4 were taken before and after the eclipse reappearance period to check for atmospheric changes and to evaluate the effect of changing air mass.

Figure 21 shows the signal as a function of time for each filter, normalized to the value 40 minutes after reappearance. This normalized signal is defined as the brightness excess, given in flux units. The magnitude of the effect at 0.4350μ is similar to that observed by Binder and Cruikshank in the B filter of the UBV system. The brightening is also apparent in the 0.5650μ filter but it is a smaller effect than that in the 0.4350μ filter.

The shape of the brightness excess vs time curve is somewhat different than most of those reported by Binder and Cruikshank, being more sharply peaked immediately after reappearance. This is probably due to the better time resolution of the present experiment, resulting from the use of the high-speed pulse-counting system.

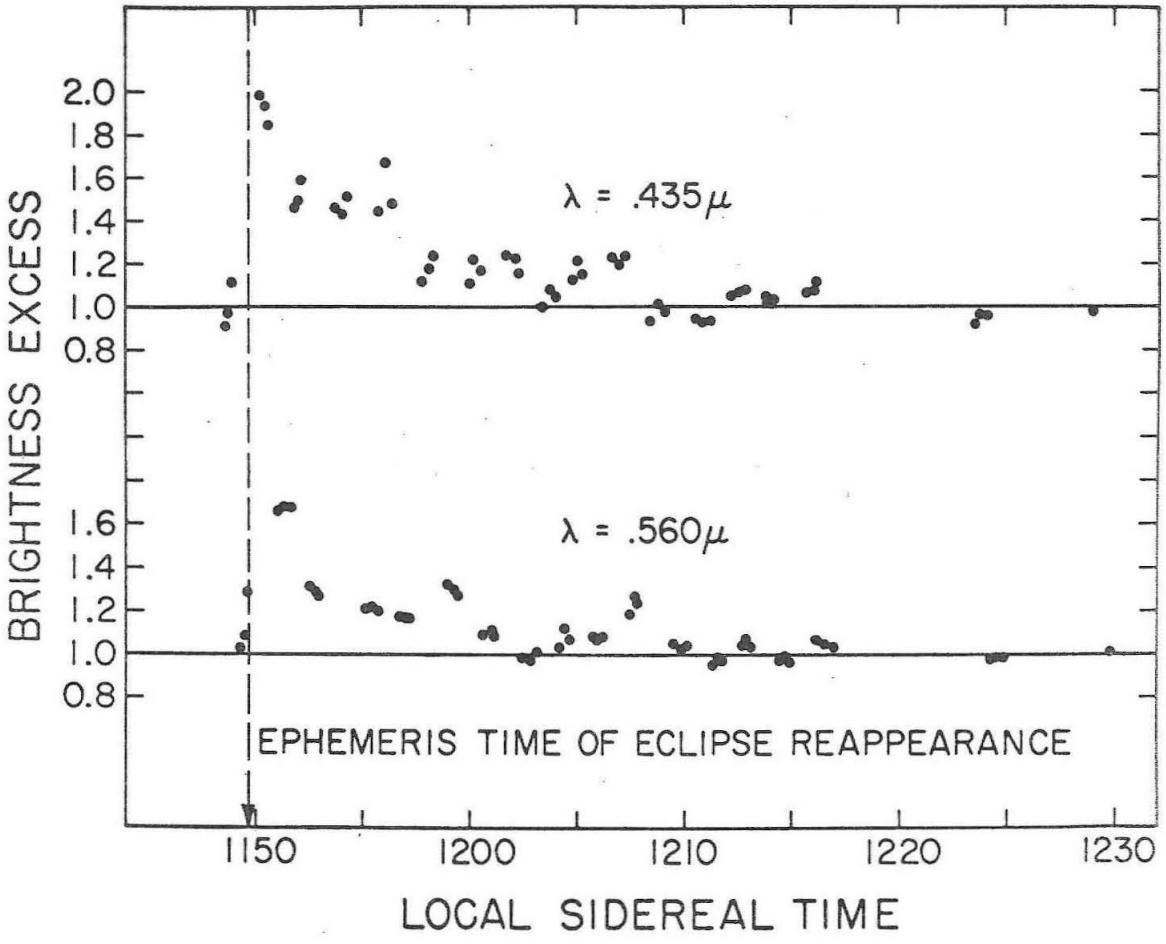

Figure 21. Brightness excess (flux normalized to normal, after eclipse reappearance, value) vs time for J1 reappearance of 1 May 1969 at 0.435μ and 0.56μ.

V. DISCUSSION

Chapter V presents a discussion of the results given in Chapter IV and of relevant work by previous researchers. This discussion is organized by topics in the following way:

Section 1). Atmospheres. This section contains a discussion of the possibility of atmospheres on the satellites in the light of theoretical studies and observational evidence.

Section 2). Surface -- Albedo. Section 2 presents a discussion of the albedos of the satellites relative to other bodies in the solar system and to laboratory studies of the albedos of silicate powders.

Section 3). Surface -- Reflectivity. This section gives a comparison between the satellite reflectivities and those of other solar system bodies. The reflectivity of silicate powders and the relationship between albedo and reflectivity are also discussed.

Section 4). Surface -- Rotational Variation. Section 4 discusses possible causes for the satellites' variation in albedo and spectral reflectivity with orbital phase and applies a simple, two-component model to the variation shown by J1.

Section 5). Eclipse Brightening. This section discusses the implications of the two-color eclipse reappearance data presented in Chapter IV and applies the model derived in Section 4 to the eclipse brightening phenomenon.

Section 6). Summary of Discussion.

Atmospheres. The only data obtained in this study which relate directly to the question of atmospheres are the J1 eclipse brightening measurements. Since the existence or absence of a volatile phase on a satellite can affect strongly the interpretation of other data, it is important to make a judgment concerning the existence and probable composition of possible satellite atmospheres. For the purposes of discussion, two cases can be defined, that of a tenuous atmosphere and that of a thick atmosphere. After Kuiper (1952), a tenuous atmosphere is one where over half of the long wavelength radiation emitted or reflected to space comes from the surface.

Thick atmospheres of elements which have spectral lines in the visible and near-infrared are ruled out for all four satellites by the upper limits placed by the spectrographic results (Kuiper, 1952). Kalinyak (1966) reported spectra of the satellites showing lines not present in the solar spectrum, but Binder and Cruikshank (1966b) suggest that they are bands of faint solar lines. The small ability of the satellites to retain gases over the age of the solar system argues against the retention of a neutral thick atmosphere, N_2 being the only common neutral species which might be retained by all of the satellites (Binder and Cruikshank, 1964).

An interesting question is the possibility of a volatile atmosphere, either too tenuous to be detected spectroscopically or composed of elements having no absorptions in the regions studied, which might exist on one or more of the satellites. The eclipse brightening phenomena of J1 and J2 observed by Binder and Cruikshank (1964, 1966a) might be explained by such an atmosphere. In their first paper they present a brief discussion of possible atmospheric constituents based on a Jeans escape model, with Kuiper's maximum subsolar temperatures (Kuiper, 1952). They conclude that the only likely constituents for tenuous

atmospheres are CH_4 and N_2 for J1, and only N_2 for J2, with H_2O being either frozen out or escaped for all four satellites. Binder and Cruikshank also mention that Sagan had pointed out that the actual escape times for N_2 and CH_4 might be shorter than those used because of exospheric heating.

Noting that the actual escape rates for N_2 and CH_4 might be higher than those they used, Binder and Cruikshank suggested that replenishment of the atmosphere is therefore implied if the eclipse brightening phenomena of J1 and J2 are actually meteorological in origin. One mechanism for replenishment is outgassing (Binder and Cruikshank, 1964); another is some form of transport from Jupiter's exosphere, which might explain the apparent decrease in eclipse brightening with distance from Jupiter (J1 brightens ~0.1 mag., J2 ~0.01 mag., and J3 has no detectable brightening).

Watson, Murray and Brown (1963), considering the problem of the stability of volatile ices (H_2O, CH_4, NH_3 and CO_2), concluded that only H_2O ice would be stable on the surface of a satellite of Jupiter. This analysis of volatile stabilities leads to the conclusion that it would be difficult for these satellites to retain even a tenuous atmosphere without some replenishment.

Another observation relative to the presence or absence of tenuous volatiles on the satellites is that of the eclipse cooling curve of J3 (Murray, Westphal and Wildey, 1965). Murray, et al, report that the entire cooling or reheating episode transpires within 15 minutes, based on observations of the 8 to 14μ flux. Combined with the visible light curve from Harris (1961), these observations imply a lag time between visible and infrared light curves of 5 minutes or less. This short lag time suggests that J3 has at least as low a thermal inertia as the moon, and the authors state that the outer few millimeters probably must be devoid of significant gas phase in order to explain this low inertia.

The temperatures of the satellites are important in determining escape rates. The infrared emission of the satellites at 10μ has been observed by Murray, Wildey and Westphal (1964). Upper limits were found for the brightness temperatures of J1 and J2. Average values of brightness temperatures were found for J3 and J4 which exceeded temperatures calculated for insulating gray bodies heated only by solar radiation. In the case of J4, the observed flux exceeded, by a factor of about 2, the flux calculated for a black body. Low (1965) has also reported 8 to 14μ brightness temperatures for the satellites; his values are somewhat lower than those of Murray, et al. Table 12 gives both sets of brightness temperatures, as well as the maximum subsolar temperatures used by Binder and Cruikshank. Since both the reduction of infrared flux observations to brightness temperatures and the calculation of theoretical fluxes are dependent on the values of the satellites' radii, the brightness temperatures are subject to serious error from this source.

Table 12. 8-14μ Brightness Temperatures

Satellite	Murray, et al	Low	T_{max}*
J1	<135	142±5	143
J2	<141	122±5	125
J3	154.5	144±5	156
J4	168.5	159±5	166

*$T_{max} = 390^{\circ} (1 - A)^{1/4} a^{-1/2}$ (Kuiper, 1952)

Jupiter's magnetic field and radiation belts are also of interest since they influence the environment of the satellites. It is known that J1, at least, modulates the decametric radiation (DAM) bursts from Jupiter (Bigg, 1964; Duncan, 1965). Binder and Cruikshank (1966a), in discussing the eclipse brightening of J2, speculated that frozen free radicals were not likely to occur on J2 since its

orbit lay outside the radiation belts of Jupiter while J1's orbit lay within them. Although J1's orbit is outside the observed limit for decimetric (DIM) radiation by 4 to 5 Jupiter radii (Warwick, 1967), it is possible that the orbit is within the outer part of the radiation belt (Duncan, 1966).

To conclude the discussion of atmospheres, it is felt that thick atmospheres are unlikely for any of the satellites. J1 and J2 probably have tenuous atmospheres, but if so, these atmospheres probably must be replenished by some mechanism. J3 almost certainly does not have even a tenuous atmosphere. There is no direct evidence for or against an atmosphere for J4, but the trend of eclipse brightening and J4's higher brightness temperature suggest that J4 has as little atmosphere as J3.

Surface -- Albedo. The geometric albedos of the satellites depend on the measured brightnesses and radii. The Bond albedos depend on the phase functions, as discussed earlier. In discussing possible surface materials for the satellites, there are two options: first, to accept the measured radii and the geometric albedos they imply, or second, to assume that the radii are not correct and that the albedos may be almost any value. For the purposes of this discussion, it will be assumed that the radii and geometric albedos of the satellites lie within the range shown in Fig. 19. The Bond albedos are very uncertain due to the extremely small range of phase angle that can be observed.

With these limitations in mind, it is interesting to compare the geometric and Bond albedos of the satellites with those of other bodies in the solar system. Table 13 lists p, q, and A for several planets and satellites (Allen, 1963), along with the p values found in this study for the Galilean satellites. Figure 19 illustrates the very high geometric albedos of the satellites relative to other solar system bodies. Indeed, the only bodies in the solar system with such high measured

geometric albedos are the smaller satellites of Saturn (whose radii are, however, even more uncertain than those of the Galilean satellites), and Venus, which has an atmosphere. These high albedos of the Galilean satellites relative to the rest of the solar system were noted by Harris (1961). It is also apparent that only very small values of q, relative to those observed for the other bodies could make the Bond albedos of J1, J2 and J3 as low as those observed for the moon, Mars, or Mercury.

Table 13. Albedos of Some Solar System Bodies

Object	p	q	A
Mercury	0.076	0.61	0.059
Mars	0.140	1.07	0.150
Moon	0.110	0.62	0.068
J1	0.778		
J2	0.782		
J3	0.604		
J4	0.261		

Thus, the Galilean satellites either have higher surface albedos than the moon, Mars or Mercury or have different phase functions. If, as has been proposed (Murray, 1969), the very low albedos of Mercury and the moon are due to saturation of some solar darkening effect, the high albedos of J1 and J2, as well as the range of albedos among the Galilean satellites, indicate that such an effect is not operating at Jupiter. This puts strong constraints on such an effect, indicating either some threshold for darkening or a very strong functional dependence on distance. Two other possible alternatives are: 1) that the satellites are protected by Jupiter's magnetosphere, or 2) that the albedos depend more on initial materials and environments than on a later darkening process.

Thus, the surfaces of the Galilean satellites are unlike much of the rest of the solar system in albedo. In order to investigate whether other known materials or some modification of known planetary surfaces can match the characteristics of the Galilean satellites, it is necessary to look at laboratory measurements. There are two categories of materials which are of particular interest for the Galilean satellites, silicate rocks and frosts.

The major way in which high albedos can be achieved is by using materials with low opacities. In studies of silicate rock powders, made by Adams and Filice (1967), it was found that basaltic rock powders, with high opacities, could not be made more than about 35% reflecting, even by reducing the grain size to below 20μ. (35% is near the lower limit for the Bond albedos of J1 and J2, assuming lunar-like phase integrals.) Since such basalts are similar to the surface materials found in the lunar mare (L.S.P.E.T., 1969), and those proposed for Mars (Adams and McCord, 1969), it seems unlikely that the surfaces of the Galilean satellites could be composed of this type of material.

Silicate powders of low opacity (Rhyolite and obsidian were used in Adam's study) may be made very bright by reducing the grain size, however. Adams and Filice found that by reducing the mean grain size to between 40 and 50μ Rhyolite tuff powders became 40-50% reflecting and obsidian became 60-70% reflecting. In each case, unsorted samples of powder had very nearly the same reflectivity as the 40-50μ size fraction.

The early analysis of the returned lunar samples (L.S.P.E.T., 1969) has indicated the presence of large amounts of glass (up to 50% of the fine grain material) in one form or another, on the lunar surface. This glass is presumably related to repeated impact events on the surface. The Galilean satellites, being near both Jupiter and the asteroid belt, may very possibly have impact rates as

high as or higher than the moon's. Thus, it is possible that the high albedos of J1, J2 and J3 may be due to the presence of large amounts of glassy material formed from low opacity silicates.

Frosts of volatiles also have high albedos, usually in the 70-90% range. However, the low stability of frosts other than H_2O frost at 5 AU, mentioned earlier, puts severe limits on possible CH_4, NH_3 or N_2 frost surfaces for the satellites, since the presence of such extensive surface deposits, unprotected by large atmospheres, would imply massive replenishment of these volatiles over the age of the solar system.

Surface -- Reflectivity. Of the previous studies of the visible reflectivity, the data collected by McNamara should be mentioned. McNamara (1964) obtained reflectivities of the satellites for 0.3175μ to 0.620μ with 12 narrowband interference filters, using G-types stars (HR 483, 16 Cyg A) to remove the solar spectrum. The overall shapes of the curves he obtained are very similar to those obtained in this study, although the slopes are slightly different, probably due to a difference between the solar spectrum used in this study and the spectra of the G stars McNamara used. When plotted with the R(0.69μ), I(0.82μ) data points from Harris (1961), the reflectivity curve for J1 given in McNamara's study shows some indication of the spectral dip between 0.5μ and 0.6μ noted in the present study. Relative spectra of J1 vs J3 taken in 1967 by McCord (personal communication) and preliminary reflectivity curves of J1 and J3 obtained by McCord and the author in 1968 also indicate this feature in J1's reflectivity curve, which had not been spectrally resolved by Harris' UBV photometry.

Little previous work in the near-infrared has been done. Moroz (1966) reported spectra of the Galilean satellites, obtained in 1963 and 1964, ranging from 0.8μ to 2.5μ. These spectra indicated that J2 and J3 had very low

reflectivities in this region, and that their reflectivities show spectral detail similar to water frost. J1 and J4 were reported to have relatively flat reflectivities in this region. Also, Kuiper has reported $2\mu/1\mu$ intensity ratios for J2 and J3 which were lower than for J1 and J4 (Harris, 1961). Considering the problems of removing the telluric water vapor absorption in this part of the spectrum and the scattered light problem when working close to Jupiter, these results should not be considered conclusive.

Comparison of spectral reflectivity curves also shows differences between the Galilean satellites and other solar system bodies, but these are not as striking as the differences in geometric albedos. Figure 22 shows the normalized reflectivity curves of J1 and J4 from this study, the lunar mare from McCord (1969), Mars dark and bright regions from McCord and Adams (1969) and a red band of Jupiter from McCord and Pilcher (1969). This figure shows that J1 and J4 (and J2 and J3, since their curves are nearly identical to J4's) do not have reflectivities which are identical to those of any of the other bodies. The lunar mare reflectivity is distinctly different from those of the satellites. Jupiter's red band curve is qualitatively similar in the 0.3μ to 0.5μ region, although generally flatter than the curves for J1 and J4; beyond 0.6μ the absorptions from methane dominate the curve. Of those curves presented, the reflectivity of the Martian dark area is perhaps closest to those of J1 and J4, but the slope of the curve from 0.4μ to 0.5μ is somewhat flatter than the slope of J1's curve.

Studies of the spectral reflectivities of silicate powders (Adams and Filice, 1967) show that the curve shapes exhibited by the Galilean satellites are within the range of those of the silicates. The type of sharp decrease in reflectivity at short wavelengths shown by J1, and, to a lesser extent, by the other Galilean

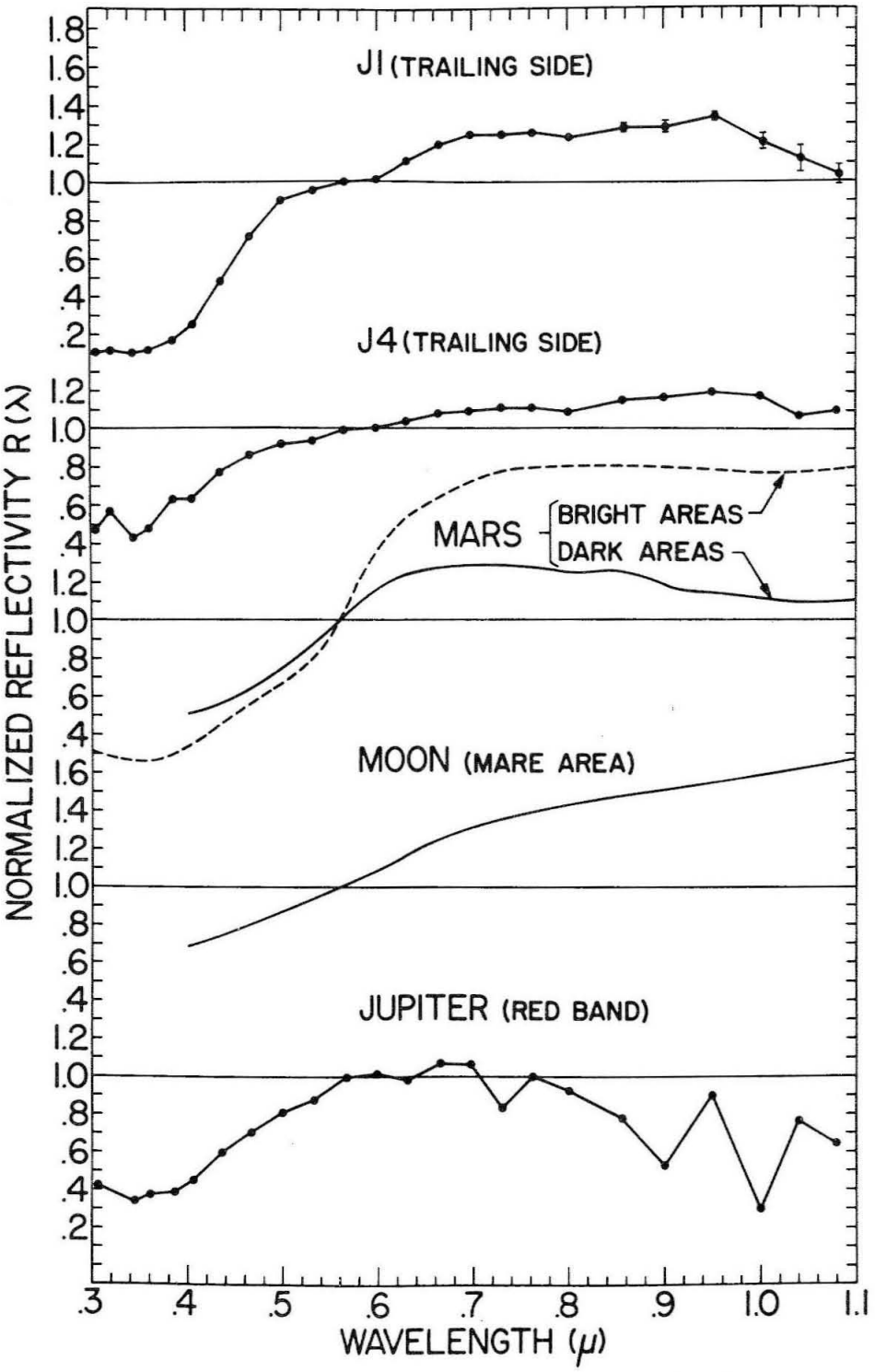

Figure 22. Spectral reflectivity for J1, J4, Mars light and dark regions, lunar mare, and a red band of Jupiter

satellites, is seen in silicates. In silicate reflectivities, this feature is probably due to the presence of Fe^{+++}(Adams, personal communication).

Laboratory data on frost reflectivities in the visible to near-infrared range are not nearly as good as the data on silicates. However, a few general comments can be made. H_2O and CO_2 frosts are essentially "white" in this part of the spectrum. Almost no data exist on CH_4 or NH_3 frosts, although such frosts appear white to the eye, probably ruling out such frosts as the main surface constituent of J1 at least. Without more experimentation, however, the possibility must remain open that frosts of this type could display reflectivity curves similar to those of the Galilean satellites under some conditions or with certain impurities.

One other aspect of the satellites' reflectivities should be noted; despite the low albedo and density of J4 relative to J2 and J3, the spectral reflectivity curves of these bodies are nearly identical. The difference in albedo between J2 and J4 is almost as large as the difference between the rest of the satellites and the moon, as Fig. 19 shows, while the reflectivities of J4 and J2 are much more similar than those of the moon and J2, or even the moon and Mars. If the similarity in spectral curves indicates similarity in surface materials, there is difficulty in explaining this difference in albedos since the addition of opaque materials or a surface effect such as radiation damage often changes the spectral curve as well as the albedo of the surface.

Particle size differences also affect the shape of the spectral curve, in a manner which depends primarily on the particle opacity. In studying silicate powders, Adams and Filice observed the ratio R/B, the ratio of reflectivity at 0.7μ to that at 0.4μ. It was found that for the less opaque materials studied, Rhyolites, obsidians and granites, the R/B ratio first increased with increasing

albedo (and therefore decreasing particle size) and then began steadily decreasing as the albedo was raised further, the turnover occurring at about 20% albedo for the samples studied, corresponding to a change in particle opacity (Adams and Filice, 1967). Because of this characteristic maximum in R/B, it is possible to have surfaces with nearly the same R/B ratio but very different albedos.

Since no work on frosts with spectral features in the visible is available, the dependence of spectral curves on albedo for these types of surfaces cannot be evaluated directly. However, the same reasoning that Adams and Filice apply to transparent powders and rock glasses should hold to first order for frosts with some visible absorbing ingredient. Such frost would then be expected to behave similarly to the Rhyolite and obsidian samples described above.

If the similarity in spectral reflectivity between J4 and J2 implies a similarity in surface materials, then the difference between their densities (Fig. 19) implies that one or both of these bodies have surfaces which are not similar to their bulk composition. That is, if J2 is a silicate body and J4 has a higher percentage of ices, then either: 1) both J2 and J4 have frost surfaces, or, 2) both have silicate surfaces, or, 3) both have some surface of some material which is not representative of either's bulk composition.

The general conclusions that one can reach on the basis of observed albedos and reflectivities of the satellites and the available laboratory data are these: first, it is difficult to make lunar- or Mars-like surfaces with albedos high enough to compare with those of J1, J2 and J3, even assuming large errors in the radii and phase integrals of these satellites; second, it is possible to make high albedo surfaces out of either low opacity silicate powders or volatile frosts; third, silicate materials with visible absorptions, probably due to Fe^{+++}, can match the

reflectivity curves of the satellites. Frosts with impurities or ingredients which absorb strongly in the short wavelength visible and ultraviolet are possible surface constituents, but no data on spectral reflectivity or stability of such materials are available at present. Jupiter's red bands, however, do exhibit curves with such low blue and ultraviolet reflectivities. Finally, it is possible to account for the range of albedos and similarity in spectral reflectivities among J2, J3 and J4 by particle size differences if the surfaces are low opacity silicates or frost which have similar absorption properties, although this process depends on the exact composition of the satellites' surfaces.

In the light of the above, the author feels that the best hypothesis at present is that the surfaces of the Galilean satellites consist of low opacity silicates, possibly with large amounts of glass; that if this is true, J1's surface probably contains silicates with more absorbing components (possibly Fe^{+++}) than the other satellites; and that J2, J3 and J4 may have very similar surface compositions, the differences in albedo possibly being due to particle size differences. If the surfaces are not silicates, the second hypothesis is that the surfaces are frosts with absorptions in the blue and ultraviolet, possibly similar to material in Jupiter's bands.

It should be noted here that the laboratory data on the changes in total spectral reflectivity with particle size and phase angle for silicates have not yet been extended to cover more than a few types of rock and that data on frosts are practically nonexistent. Also, the very important spectral region from 1μ to 2μ has not been observed in detail for the satellites except for the observations reported by Moroz (1966).

Surface -- Rotational Variation. The satellites' variation in brightness and spectral reflectivity with orbital phase angle provides additional clues to surface composition and processes. The narrowband photometry presented in this study indicates systematics in both brightness and spectral variations which were not obvious in earlier broadband work. First, it is usually stated that the leading sides of J1, J2 and J3 are brighter than the trailing sides (Harris, 1961). That this is only approximately true can be seen by close examination of the V magnitude variation given by Harris or of the light curves at 0.56μ presented in Figs. 14-17. Such examination shows that J1 remains high in brightness until well after θ = 180 deg, the light curve dropping sharply to its minimum at about θ = 300 deg. J2, on the other hand, begins to decrease in brightness somewhat before 180 deg, falling to a much broader minimum just short of 300 deg. J3's light curve has begun to decline by θ = 120 deg and actually appears to have its minimum just beyond 180 deg. J4, away from α = 0, has a minimum in its light curve short of 180 deg. The spectral variations of J1 and J2, for which detailed variations with θ in spectral reflectivity were observed, seem to be in phase with the light curves.

Figure 23 gives the rotational angle of the point where the light curve crosses the mean value as a function of distance from Jupiter for the four satellites. The error bar is derived from the spread in mean crossings between the extreme variations of A given in Figs. 14-17. The variation shown illustrates that no simple separation of "leading side" and "trailing side" effects completely describes the observations.

The spectral form of the orbital variation, given in the preceding chapter, is very similar for all four satellites, the differences between them being primarily the exact position of the ultraviolet-blue variation and the presence or absence of

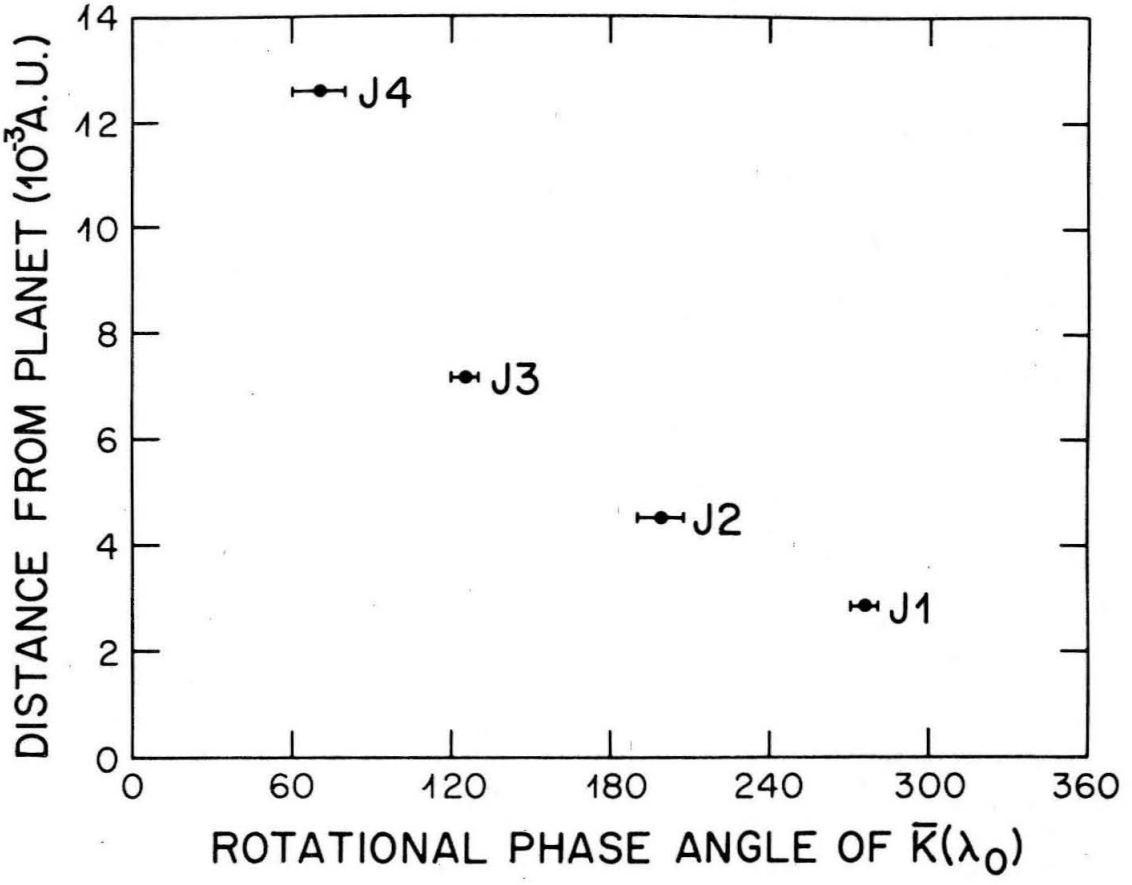

Figure 23. Value of θ at which the light curve crosses $\overline{K(\lambda_0)}$ between 0 and 360 deg, as a function of the satellites' distance from Jupiter.

a variation in the red part of the spectrum. This similarity in the satellites' orbital variation strongly suggests that the process or processes involved in the variation may be the same on each satellite. This is compatible with, but not proof of, similar surface compositions for the satellites.

Several possible explanations for the rotational variation of the satellites exist. Probably the most straightforward of these is that the satellites have areas, or spots, of different composition on their surfaces. Such a theory was mentioned by Harris (1961). The visual descriptions of dark and light areas on the satellites and the fact that other solar system bodies, the moon and Mars in particular, have such regions of apparently different composition are support for this theory. The similarity in variation among the satellites and the connection between brightness and spectral variations indicates that, if such compositional differences exist, they are similar on all the satellites. The systematic variation of the brightness with θ shown in Fig. 23 suggests that some type of connection between surface composition and the dynamics of the satellite's orbit may be present, as is the case with the moon's synchronous rotation and the distribution of mare areas.

A possible explanation which is similar to the above compositional hypothesis is a change in the texture or age of the satellites' surfaces from side to side. Either effect might alter the spectral curve of the surface. The above remarks on non-random distribution apply here as well as to the compositional discussion.

Meteorological explanations for the rotational variation have also been advanced, particularly the possibility of a morning limb arc which persists on the leading side (Firsoff, 1968). The regularity of the rotational variation and its similar form for all the satellites, despite evidence of different degrees of atmospheric phenomena (eclipse brightening and eclipse cooling, for instance) among

the satellites, tend to argue against a meteorlogical source for the rotational variation. However, some combination of frost with compositional differences, possibly due to an associated temperature difference cannot be ruled out at present.

Comment should be made here on the possibility that something in the near environment of Jupiter is directly responsible for the variation in spectral curves and brightness of the satellites. Such an effect is considered unlikely for two major reasons. First, the satellites show a maximum of brightness and spectral change at different points in their orbits relative to Jupiter. Second, the rotation period of Jupiter is shorter than the orbital period of any of the satellites. Therefore, the same orbital phase angle would not correspond to the same position relative to Jupiter's "surface" or magnetic field even on two successive revolutions.

In order to investigate more completely the effects of compositional variations, frosts, or particle size differences on the spectral reflectivities and albedos of the satellites, it is useful to construct a simple model for the reflectivity of a mixture of two materials. It is assumed that the albedos of the two components, $A(\lambda)$ and $B(\lambda)$, will affect the albedo of the mixture, $C(\lambda)$, in proportion to the fraction of the surface covered by each. Thus, if a fraction, X, of the surface is $B(\lambda)$ and $(1 - X)$ is $A(\lambda)$, $C(\lambda)$ is given by Equation 22:

$$22). \quad C(\lambda) = XB(\lambda) + (1 - X)A(\lambda)$$

To put this equation in terms of measured quantities, the normalized reflectivities $R_A(\lambda)$, $R_B(\lambda)$, $R_C(\lambda)$ and the ratios of C and B to A at λ_0 are used. The ratios of C and B to A at λ_0, α, and β are defined by:

$$23). \quad \alpha = \frac{C(\lambda_0)}{A(\lambda_0)} \quad ; \quad \beta = \frac{B(\lambda_0)}{A(\lambda_0)}$$

Using the definition of $R_i(\lambda)$, the normalized reflectivity of component i, in the form:

$$24). \quad R_i(\lambda) = \frac{i(\lambda)}{i(\lambda_0)}$$

and dividing Equation 22 by $A(\lambda_0)$, we obtain:

$$25). \quad \alpha R_C(\lambda) = \beta X R_B(\lambda) + (1 - X) R_A(\lambda)$$

Evaluating this equation at $\lambda = \lambda_0$, where the reflectivities are unity, an expression for X in terms of α and β is obtained:

$$26). \quad X = \frac{\alpha - 1}{\beta - 1}$$

Using this relation, Equation 25 can be written as:

$$27). \quad R_C(\lambda) = (1 - \frac{\beta X}{\alpha}) R_A(\lambda) + \frac{\beta X}{\alpha} R_B(\lambda)$$

Applying this model to the satellites, $R_A(\lambda)$ becomes the reflectivity of the dark side, $R_C(\lambda)$ the reflectivity of the bright side, and $R_B(\lambda)$ the reflectivity of some hypothetical component which must be added in fraction X to the dark side in order to produce the bright side. α, then, is the observed ratio of brightness at λ_0, between the bright and the dark side, and β is the ratio of the unknown material to the dark side at λ_0. Since X, β, and α are related by Equation 26, and since α is known, it is only necessary to choose either β or X in order to solve Equation 27 for $R_B(\lambda)$, the unknown reflectivity.

As an example, the model is applied to J1, which has the largest spectral rotation effect. Since J1's geometric albedo is high to begin with, some limits can be placed on β's for realistic materials. Taking $p(\lambda_0) = 0.7$ for the geometric albedo of the dark side, for the mean radius (see Fig. 19), β's greater than 2,

corresponding to a geometric albedo >1.4 for the unknown material were not considered. $R_B(\lambda)$'s were found for three different combinations of $R_C(\lambda)$ and α, taken at different θ's, using the same $R_A(\lambda)$. Figure 24 shows these three $R_B(\lambda)$ curves for each of three different values of β.

The curves in Fig. 24 illustrate three cases. The first case is shown in the lower curves. These curves indicate that for small β's, fairly large areas of the surface (20-60%) must be covered with a material with a reflectivity very similar to the reflectivity of the dark side, but somewhat less absorbing in the blue. This case corresponds physically to a large percentage of the satellite's surface being covered with a material very similar in reflectivity and only slightly higher in albedo than the dark side. Such a difference could be accounted for by particle size difference or some minor surface alteration.

The second case, illustrated by the middle curves, shows that, for a β giving a near unity geometric albedo for the unknown component, 5-15% of the surface must be covered with a material having a relatively flat reflectivity from 0.4μ to 0.95μ, with a sharp drop for $\lambda \leq 0.4\mu$. Unfortunately, only one curve in the ultraviolet is available, so there is no confirmation of the apparently sharp drop in $R_B(\lambda)$ shown. Case 2 represents the presence on the satellite's bright side of relatively small amounts of very bright material which is gray from 0.4μ to 0.95μ. This case implies that the added component may have a different composition, perhaps frost, if the drop in the ultraviolet is not real.

The third case indicates that, for $\beta \sim 2$, 1-6% of the surface must be covered by material with a reflectivity which has a nearly 40% drop from 0.4μ to 0.95μ. Again the drop in the ultraviolet is unconfirmed. This is an extreme case of a very small area on the satellite being covered with a very bright substance.

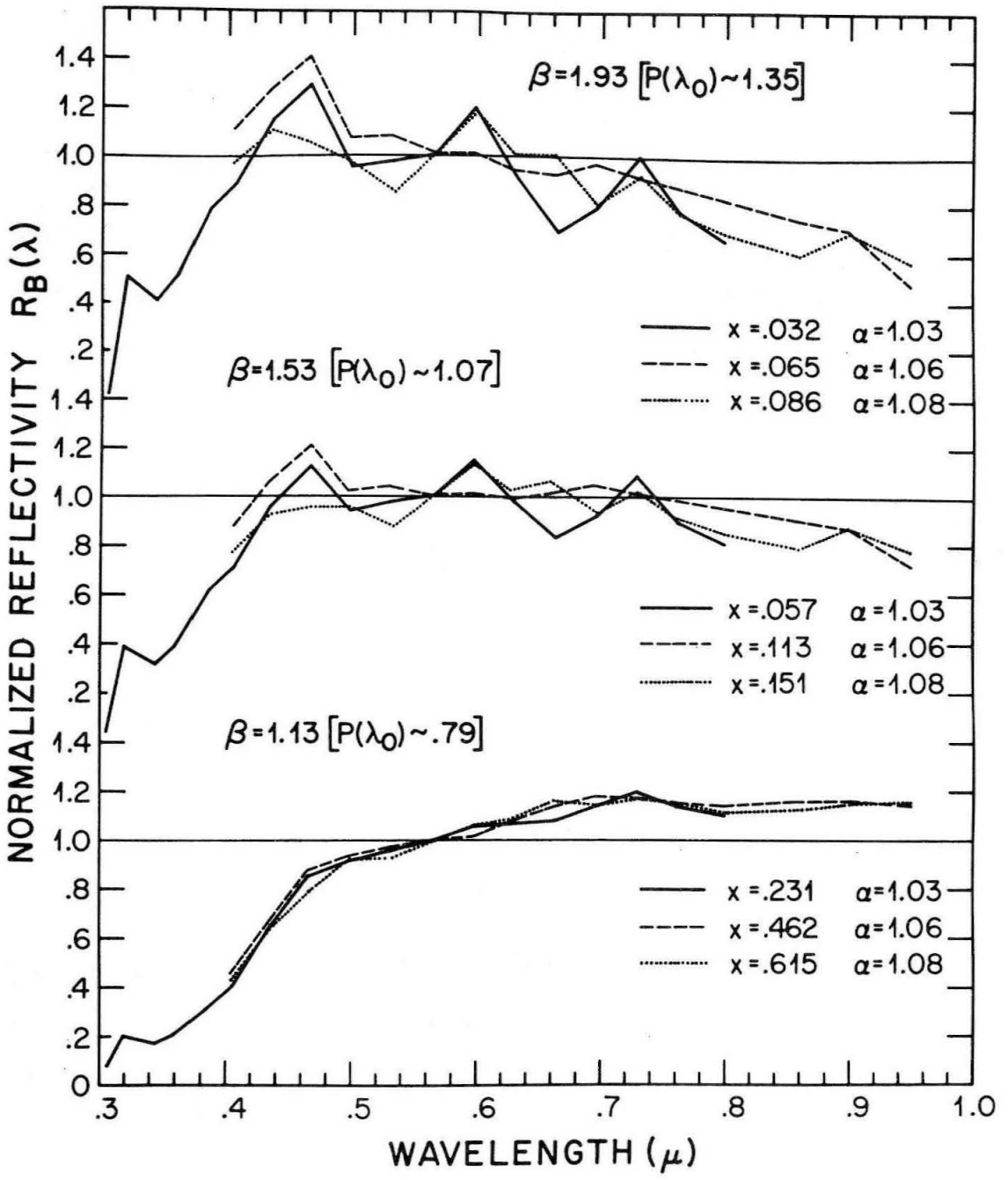

Figure 24. $R_B(\lambda)$, the spectral reflectivity of the second component, for several α, β, and X combinations.

This case shows that, for $\beta \geq 2$, not only does the albedo become unrealistically high, but the $R_B(\lambda)$ curves also tend to become more extreme and unrealistic.

To summarize, investigation of a two-component model indicates that in order to match the rotational variation in albedo and spectral reflectivity observed for J1, it is necessary to assume that a fraction of one side of the satellite is covered by a material with a higher albedo and a different spectral reflectivity than the other side. The model also indicates that for realistic values for the albedo of the bright fraction, the spectral reflectivity of this fraction must be qualitatively similar to that of the other side. Such differences in spectral reflectivity might be caused by particle size differences or a change in the amount of the absorbing material. The addition of a fraction of bright, gray material (such as H_2O frost) does not seem compatible with any of the cases presented, although Case 2 above is close if the drop in the ultraviolet is not real.

It should be noted again that the model presented here is very simple. It presents only a two-component system, and assumes that the fraction, X, of component B, varies as the projected area of B for a spherical surface. A three-component system produces non-unique solutions since the albedo and reflectivity of two of the components are then unknowns.

Eclipse Brightening. The observation of eclipse brightening at two wavelengths, reported in the previous chapter, not only confirms the existence of this phenomenon but also provides further information about the possible cause of the brightening. Binder and Cruikshank (1964) calculated the percent of surface that must be covered by a frost with 0.8 albedo in order to give the observed brightening at 0.455μ. Such a frost would not be bright enough to account for the brightness excess $\sim$1.7 at 0.56μ (see Fig. 21) if J1 has a geometric albedo greater than 0.47, which it almost certainly does (see Fig. 19).

Furthermore, the change in the $0.435\mu/0.56\mu$ ratio, given by the differing brightness excesses at these two wavelengths, allows the use of the model of the previous section to calculate the $R_B(0.435\mu)$ of the material supposed to have been deposited during the eclipse. The normalized reflectivity for J1 at 0.435μ is about 0.49. This is taken as $R_A(0.435\mu)$ in Equation 27. The increase in $R(0.435\mu)$ at the time of maximum brightness excess is a factor of 1.13. This yields $R_C(0.435\mu) = 0.554$. The brightness excess at 0.56μ yields $\alpha = 1.68$. $R_B(0.435\mu)$ can then be calculated for different choices of β (and therefore X).

Table 14 gives several values of $R_B(\lambda = 0.435\mu)$ for various β values, along with the X and $p(\lambda = 0.56\mu)$ values for the added material.

Table 14. $R_B(\lambda = 0.435\mu)$ for Various β Values

β	X	$p(\lambda = 0.56\mu)$	$R_B(\lambda = 0.435\mu)$
2.0	0.68	1.56	0.570
2.5	0.45	1.95	0.585
3.0	0.34	2.34	0.595

Thus, if the brightness excess at 0.56μ is real, the material which must be added to the surface to explain it must not only have a high geometric albedo, but also have a decrease in reflectivity toward the shorter wavelengths, as shown by the $R_B(\lambda = 0.435\mu)$ values. Further observations of eclipse brightening at many wavelengths are needed to resolve this problem.

Summary of Discussion. The following statements summarize the major conclusions reached in this chapter. 1) None of the satellites is felt to possess optically thick atmospheres. 2) J1 and J2 probably have tenuous atmospheres, which may imply some replenishment of volatiles for these satellites over the age of the solar system. 3) J3 and J4 probably do not possess even tenuous

atmospheres. 4) The albedos of the satellites' surfaces are almost certainly not lunar-like or Mars-like. 5) The reflectivities of the satellites' surfaces are not identical to those of the moon, Mars or Jupiter, but they are qualitatively similar in some respects to the curves for Mars and Jupiter. 6) Surfaces of either low opacity silicates, possibly glassy in form, or frosts with ingredients which absorb in the blue and ultraviolet are necessary to explain the high albedos and reflectivity curves of the satellites. However, the existence of frosts would raise theoretical problems in view of the low stability of most frost species at Jupiter's heliocentric distance. 7) The similarity in rotational variation among the satellites suggests that this variation is caused by similar processes on each of the satellites. 8) Investigation of a two-component model for J1's rotational variation yields two likely cases. The first case has large areas of the surface covered by material differing only slightly in albedo and reflectivity from the rest of the surface, possibly due to particle size differences. The second case involves small areas of the surface covered by material significantly brighter than the rest of the surface and having a different reflectivity curve, probably implying a different composition. 9) The observation of eclipse brightening at both 0.435μ and 0.56μ implies a very bright ($p>1$), colored deposit, if the brightening is meteorological in origin. This observation needs to be confirmed at several wavelengths before firm conclusions can be drawn.

VI. FUTURE WORK

Since the major part of the rotational spectral variation appears to occur in the ultraviolet for J2, J3 and J4, more orbital phase coverage in the ultraviolet is needed, not only to confirm these variations, but also to supply more information about the variation with θ. Special attention should be given to confirming J4's phase law and to searching for a possible change in spectral variation with solar phase. More observations close to opposition should be made to determine the phase laws of the satellites more accurately and to look for a possible "opposition effect".

Another extension of the present work that is needed is an increase in the spectral range covered. Observations between 1 and 2μ (where many important absorptions occur in some silicates and frosts) would be very useful, both in confirming Moroz's work and in the possible discovery of rotational variations in this spectral range.

Laboratory work on frosts and further work on silicate powders is also needed. In particular, the dependence of albedo and spectral reflectivity on particle size should be investigated.

The wavelength dependence of the eclipse brightening phenomena may be very useful in understanding the cause of the phenomena and the possible substances involved. Therefore, confirmation of the eclipse brightening effect on J1 at 0.56μ and the extension of these observations to several other wavelengths should have a high priority during the next opposition. A search for similar effects on the other satellites, particularly J2, should also be made. Also,

concerning the question of possible satellite atmospheres, eclipse cooling curves for all the satellites should be obtained as soon as possible.

Since the Bond albedos of the satellites are very important in determining surface composition and condition, accurate radii and phase laws are needed. While it may be possible to obtain better measurements of the radii from better earth-based or earth-orbital observations, the phase laws can be practically determined only by a fly-by, unmanned spacecraft mission. Both radii and the phase laws could be determined by a relatively simple photometric system on such a fly-by spacecraft. Since this basic information is important to the design of more complicated experiments to investigate the satellites, an attempt to determine radii and phase laws should be made at the earliest opportunity. If the system used for taking these measurements is an imaging system, first order information on the distribution of surface materials, the history of cratering, and the existence of tenuous atmospheres might also be obtained.

APPENDIX A

APPENDIX A

This appendix contains a computer listing of the basic data for determining the albedo at 0.56μ. For each date there is a card giving the date, the solar phase angle (immediately after the date for all but 03/01/69), the sun-Jupiter distance, the earth-Jupiter distance, the number of filters used, and the filter number of the 0.56μ filter. Following this card is a card for each satellite observed on this date, listing the date, the satellite, the average observed ratio of the satellite flux to o Virgo flux at 0.56μ, the standard deviation of the average, the average satellite/o Virgo ratio corrected for r, Δ, and phase law (called $K(\lambda_0, \theta)$ in the text), the standard deviation of the average for this quantity, the number of observations of the satellite, and finally, the average orbital phase angle for the satellite on that date.

```
3/01/69 3.98   5.4455   4.5161 18  9
3/01/69  J1  0.322491E 00  0.117311E-02  0.475856E 00  0.173100E-02  9 254.5
3/01/69  J2  0.236491E 00  0.369077E-03  0.329326E 00  0.513959E-03  6 262.0
3/01/69  J4  0.168041E 00  0.679454E-03  0.271826E 00  0.109910E-02  8 320.0
03/04/693.42   5.4458   4.4987 18  9
03/04/69 J1  0.355885E 00  0.150316E-02  0.510861E 00  0.215773E-02  6 125.0
03/04/69 J2  0.258957E 00  0.361979E-03  0.353839E 00  0.494608E-03  2 203.0
03/04/69 J3  0.475163E 00  0.253016E-02  0.656095E 00  0.349359E-02  3 146.0
03/04/69 J4  0.173903E 00  0.263101E-02  0.270979E 00  0.409969E-02  2  25.0
03/05/693.23   5.4459   4.4935 18  9
03/05/69 J1  0.312000E 00  0.000000E 00  0.442000E 00  0.000000E 00  1 320.0
03/10/692.25   5.4463   4.4718 18  9
03/10/69 J1  0.325670E 00  0.370028E-02  0.442352E 00  0.502602E-02  8 278.0
03/10/69 J2  0.301059E 00  0.304742E-02  0.396110E 00  0.400956E-02  4  88.0
03/10/69 J3  0.515474E 00  0.622283E-02  0.681832E 00  0.823111E-02  6  88.0
03/10/69 J4  0.180869E 00  0.911701E-03  0.260395E 00  0.131256E-02  4 153.0
03/11/692.05   5.4464   4.4684 18  9
03/11/69 J1  0.358839E 00  0.158051E-02  0.482947E 00  0.212715E-02  9 121.0
03/11/69 J2  0.276442E 00  0.273252E-02  0.361450E 00  0.357277E-02  2 195.0
03/11/69 J3  0.490220E 00  0.171789E-02  0.643915E 00  0.225648E-02  8 139.0
03/11/69 J4  0.176593E 00  0.434033E-02  0.250777E 00  0.616363E-02  3 173.5
03/22/690.0    5.4473   4.4509 18  9
03/22/69 J1  0.373313E 00  0.504217E-02  0.458968E 00  0.619907E-02  4 209.0
03/22/69 J2  0.277337E 00  0.926118E-03  0.340970E 00  0.113861E-02  7 223.0
03/22/69 J3  0.540634E 00  0.940852E-03  0.664680E 00  0.115673E-02  3 330.0
03/22/69 J4  0.223662E 00  0.752505E-03  0.274980E 00  0.925164E-03  7  55.0
03/23/690.51   5.4473   4.4512 18  9
03/23/69 J1  0.362804E 00  0.754105E-02  0.455740E 00  0.947275E-02  5  35.0
03/23/69 J2  0.258262E 00  0.182288E-02  0.322151E 00  0.227382E-02  6 320.0
03/23/69 J3  0.568479E 00  0.513111E-02  0.709587E 00  0.640476E-02  8  15.0
03/23/69 J4  0.215778E 00  0.328585E-02  0.275041E 00  0.418831E-02 10  74.0
03/26/691.08   5.4475   4.4539 18  9
03/26/69 J1  0.363278E 00  0.232267E-02  0.467720E 00  0.299043E-02  4 250.0
03/26/69 J4  0.201930E 00  0.256897E-04  0.267892E 00  0.340814E-04  3 136.5
04/10/694.00   5.4487   4.5082 18  9
04/10/69 J1  0.330913E 00  0.217319E-02  0.487470E 00  0.320134E-02  7  93.0
04/10/69 J2  0.259561E 00  0.116450E-02  0.360879E 00  0.161842E-02  2 340.0
04/10/69 J3  0.444705E 00  0.204399E-02  0.626536E 00  0.287973E-02  4 208.0
04/10/69 J4  0.159981E 00  0.101549E-02  0.258445E 00  0.164049E-02  6 104.0
04/11/694.18   5.4487   4.5141 18  9
04/11/69 J1  0.342000E 00  0.753514E-02  0.466000E 00  0.111996E-01  4 275.0
04/11/69 J2  0.292000E 00  0.111310E-01  0.408000E 00  0.155651E-01  2  83.0
04/11/69 J3  0.499214E 00  0.896251E-02  0.708415E 00  0.127183E-01  2 252.0
04/11/69 J4  0.156853E 00  0.144829E-02  0.256417E 00  0.236760E-02  4 123.5
04/13/694.55   5.4489   4.5268 19  6
04/13/69 J1  0.289093E 00  0.549820E-02  0.437652E 00  0.832362E-02  3 325.0
04/13/69 J2  0.224486E 00  0.198498E-02  0.317889E 00  0.281088E-02  2 295.0
04/13/69 J4  0.151214E 00  0.144772E-02  0.253231E 00  0.242443E-02  4 168.0
04/16/695.09   5.4491   4.5479 18 11
04/16/69 J1  0.305119E 00  0.173825E-02  0.474772E 00  0.270476E-02  6 228.0
04/16/69 J2  0.239020E 00  0.211529E-02  0.344927E 00  0.305255E-02  5 235.0
04/16/69 J3  0.451420E 00  0.237933E-02  0.665043E 00  0.350529E-02  6 148.0
04/16/69 J4  0.162465E 00  0.869845E-03  0.281771E 00  0.150861E-02  6 232.0
04/17/695.26   5.4491   4.5555 19  6
04/17/69 J1  0.312718E 00  0.365502E-02  0.490951E 00  0.573818E-02  2  75.0
04/17/69 J2  0.231308E 00  0.0           0.335869E 00  0.417806E 29  1 339.0
04/17/69 J3  0.431244E 00  0.0           0.640044E 00 -0.911226E-76  1 202.0
04/17/69 J4  0.158061E 00  0.554025E-03  0.277192E 00  0.971596E-03  2 256.0
04/18/695.43   5.4492   4.5633 18 11
04/18/69 J1  0.291198E 00  0.292589E-02  0.461303E 00  0.463507E-02  5 273.0
04/18/69 J2  0.282191E 00  0.390500E-03  0.412333E 00  0.570590E-03  2  77.0
```

```
04/18/69 J3  0.432186E 00  0.273451E-02  0.646295E 00  0.408921E-02  2 250.0
04/18/69 J4  0.156721E 00  0.106841E-02  0.277912E 00  0.189460E-02  5 277.0
04/20/695.78  5.4493  4.5797 19  6
04/20/69 J1  0.275702E 00  0.911149E-02  0.444886E 00  0.147027E-01  2 328.0
04/20/69 J4  0.150260E 00  0.0           0.272510E 00 -0.390868E-59  1 316.0
04/21/695.94  5.4494  4.5883 19  6
04/21/69 J1  0.307048E 00  0.321200E-02  0.499854E 00  0.522893E-02  2 152.0
04/21/69 J2  0.239160E 00  0.0           0.356149E 00  0.417806E 29  1  19.0
04/21/69 J3  0.456415E 00  0.169202E-02  0.698378E 00  0.258903E-02  3  41.0
04/21/69 J4  0.144849E 00  0.177371E-02  0.265478E 00  0.325082E-02  3 340.0
04/22/696.10  5.4495  4.5971 19  6
04/22/69 J1  0.267290E 00  0.987097E-02  0.439006E 00  0.162124E-01  2 340.0
04/22/696.10  5.4495  4.5971 18 11
04/22/69 J2  0.270021E 00  0.146902E-02  0.404624E 00  0.220131E-02  2 118.0
04/22/69 J3  0.458315E 00  0.298101E-02  0.706606E 00  0.459595E-02  2  90.0
04/22/69 J4  0.132843E 00  0.0           0.246041E 00 -0.589244E-76  1   4.4
04/29/697.18  5.4499  4.6654 18 11
04/29/69 J1  0.266000E 00  0.200000E-01  0.465000E 00  0.400000E-01  4 334.0
04/29/69 J2  0.263157E 00  0.801854E-03  0.412136E 00  0.125580E-02  6 105.0
04/29/69 J3  0.443913E 00  0.142134E-02  0.722247E 00  0.231253E-02  7  82.0
04/29/69 J4  0.130354E 00  0.186402E-02  0.259199E 00  0.370647E-02  9 154.0
05/12/698.82  5.4504  4.8183 19  6
05/12/69 J1  0.261907E 00  0.202703E-02  0.510996E 00  0.395485E-02  4 100.0
05/12/69 J2  0.193273E 00  0.0           0.328434E 00  0.406683E-55  1 340.0
05/12/69 J3  0.367404E 00  0.0           0.659975E 00  0.219727E-02  1 151.9
05/12/69 J4  0.119421E 00  0.103429E-02  0.266749E 00  0.231029E-02  3  75.0
05/13/698.92  5.4507  4.8313 19  6
05/13/69 J1  0.209234E 00  0.149511E-02  0.411536E 00  0.294068E-02  3 300.0
05/13/69 J3  0.372813E 00  0.0           0.674708E 00 -0.657165E 20  1  63.3
05/13/69 J4  0.106970E 00  0.238881E-02  0.240900E 00  0.537968E-02  3  96.0
```

REFERENCES

Adams, J. B. and A. L. Filice. "Spectral Reflectance 0.4 to 2.0 Microns of Silicate Powders," J. Geophys. Res., 72, No. 22, pp. 5705-5715, (1967).

Adams, J. B. and T. B. McCord. "Mars: Interpretations of Spectral Reflectivity of Light and Dark Regions," J. Geophys. Res., 74, pp. 4851-4856, (1969).

Allen, C. W. (ed.). Astrophysical Quantities, 2nd ed. University of London, The Athlone Press (1963).

Binder, A. B. and D. P. Cruikshank. "Evidence for an Atmosphere on Io," Icarus, 3, pp. 299-305, (1964).

_____. "Photometric Search for Atmospheres on Europa and Ganymede, Icarus, 5, pp. 7-9, (1966a).

_____. "On the Spectra of the Galilean Satellites of Jupiter," Ap. J., 144, No. 3, p. 1240, (1966b).

Bigg, E. K. Nature, 203, p. 1088, (1964).

Code, A.D. "Stellar Energy Distribution" in Stellar Atmospheres, Jesse L. Greenstein, ed., University of Chicago Press, p. 50, (1960).

Duncan, R. A. "Modulation of Jupiter's Decametric Emission by the Satellite Io," Planet. Space Sci., 13, p. 997, (1965).

_____. "Comments of the Modulation of Jovian Decametric Emission by Jupiter's Satellites," Planet. Space Sci., 14, No. 2, p. 173, (1966).

Firsoff, Vlademar A. Exploring the Planets, (Rev. ed.). A.S. Barnes & Co., S. Brunswick, N.J. and New York, p. 149, (1968).

Hapke, Bruce and Hugh Van Horn. "Photometric Studies of Complex Surfaces, with Applications to the Moon," J. Geophys. Res., 68, No. 15, p. 4545, (1963).

Harris, Daniel L. "Photometry and Colorimetry of the Planets and Satellites," in The Solar System, Vol. III: Planets and Satellites. Gerard P. Kuiper and Barbara M. Middlehurst, eds., University of Chicago Press, p. 272, (1961).

Kalinyak, A.A. "Data on the Spectra of the Galilean Satellites of Jupiter," Soviet Astronomy A J, 9, No. 5, pp. 824-825, (1966).

Kuiper, G. P. (ed.) The Atmospheres of the Earth and Planets (Rev. ed.). The University of Chicago Press, (1952).

Lambert, D. personal communication, (1967).

Low, Frank J. "Planetary Radiation at Infrared and Millimeter Wavelengths," Lowell Observatory Bulletin No. 128, VI, No. 9, p. 184, (1965).

Lunar Samples Preliminary Examination Team. "Preliminary Examination of Lunar Samples from Apollo 11," Science, 165, p. 1211, (1969).

McCord, Thomas B. "A Double Beam Astronomical Photometer," Ap.Op., 7, No. 3, pp. 475-478, (1968).

_____. "Spectral Reflectivity of the Moon," in preparation, (1969).

McCord, T. B. and J. B. Adams. "Spectral Reflectivity of Mars," Science, 163, pp. 1058-1060, (1969).

McCord, T. B. and C. Pilcher. "Reflectivity of Bands of Jupiter," in preparation, (1969).

McNamara, D. H. "Narrowband Photometry of Stars, Planets and Satellites," North American Aviation, Inc., Space and Information Systems Division, SID 64-78, Accession No. 52156-64, (1964).

Michelson, A. A. "Measurements of Jupiter's Satellites by Interference," Nature, 45, p. 160, (1891).

Moroz, V. I. "IR Spectrophotometry of the Moon and Galilean Satellites of Jupiter," Soviet Astronomy A J, 9, No. 6, p. 999, (1966).

Murray, B. C. personal communication, (1969).

Murray, B. C., J. A. Westphal, and R. L. Wildey. "The Eclipse Cooling of Ganymede," Ap. J., 141, No. 4, pp. 1590-1592, (1965).

Murray, B. C., R. L. Wildey, and J. A. Westphal. "Observations of Jupiter and the Galilean Satellites at 10 Microns," Ap. J., 139, No. 3, pp. 986-993, (1964).

Oetking, Philip. "Photometric Studies of Diffusely Reflecting Surfaces with Applications to the Brightness of the Moon," J. Geophys. Res., 71, No. 10, pp. 2505-2515, (1966).

Oke, J. B. "Photoelectric Spectrophotometry of Stars Suitable for Standards," Ap. J., 140, No. 2, p. 689, (1964).

Porter, J. G. "The Satellites of the Planets," JBAA, 70, pp. 33-59, (1960).

Robinson, Nathan (ed.). Solar Radiation. Elsevier Publishing Co., Amsterdam, New York, (1966).

Sharonov, V. V. The Nature of the Planets. (1958). Translated by Israel Program for Scientific Translations, (1964).

Stebbins, J. Lick Observatory Bulletin, No. 385, (1927).

Stumpff, K. "Über die Albedo der Planeten und die photometrische Bestimmung von Planetoidendurchmesser," Astron. Nachr., 276, No. 3, pp. 118-126, (1948).

Van Diggelen, J. "The Radiance of Lunar Objects near Opposition," Planet. Space Sci., 13, No. 4, p. 271, (1965).

Warwick, J. W. "Radiophysics of Jupiter," Space Science Reviews, VI, No. 6, p. 841, (1967).

Watson, K., B. C. Murray, and H. Brown. "Stability of Volatiles in the Solar System," Icarus, 1, No. 4, pp. 317-327, (1963).